https://doi.org/10.5194/egusphere-2023-160
Preprint. Discussion started: 8 March 2023

Modelling the impacts of emission changes on O_3 sensitivity, atmospheric oxidation capacity and pollution transport over the Catalonia region

Alba Badia[1], Veronica Vidal[1,2], Sergi Ventura[1], Roger Curcoll[3], Ricard Segura[1], and Gara Villalba[1,4]

[1]Sostenipra Research Group, Institute of Environmental Sciences and Technology, Universitat Autònoma de Barcelona, 08193 Bellaterra, Barcelona, Spain.
[2]Departament d'Arquitectura de Computadors i Sistemes Operatius (CAOS), Escola d'Enginyeria, Universitat Autònoma de Barcelona 08193 Bellaterra, Barcelona, Spain.
[3]Institut de Tècniques Energètiques (INTE), Universitat Politècnica de Catalunya, Barcelona, Spain
[4]Department of Chemical, Biological and Environmental Engineering, Universitat Autònoma de Barcelona, 08193 Bellaterra, Barcelona, Spain

Correspondence: alba.badia@uab.cat

Abstract. Tropospheric ozone (O_3) is an important surface pollutant in urban areas, and it has complex formation mechanisms that depend on the atmospheric chemistry and meteorological factors. The severe reductions observed in anthropogenic emissions during the COVID-19 pandemic can further our understanding of the photochemical mechanisms leading to O_3 formation and provide guidance for policies aimed at reducing air pollution. In this study, we use the air quality model WRF-Chem coupled with the urban canopy model BEP-BEM to investigate changes in the ozone chemistry over the Metropolitan Area of Barcelona (AMB) and its atmospheric plume moving northwards, which is responsible for the highest number of hourly O_3 exceedances in Spain. The trajectories of the air masses from the AMB to the Pyrenees are studied with the Lagrangian particle dispersion model FLEXPART-WRF. The aim is to investigate the response of ozone chemistry to changes in the precursor emissions. The results show that with the reduction in emissions: 1) the ozone chemistry tends to enter the NOx-limited or transition regimes; however, highly polluted urban areas are still in the VOC-limited regime, 2) the reduced O_3 production is overwhelmed by reduced nitric oxide (NO) titration, resulting in a net increase in the O_3 concentration (up to 20%) in the evening, 3) the increase in the maximum O_3 level (up to 6%) during the lockdown could be attributable to an enhancement in the atmospheric oxidation capacity (AOC), 4) the daily maximum levels of ozone and odd oxygen species (O_x) generally decreased (4%) in May with the reduced AOC, indicating an improvement in the air quality, and, 5) ozone precursor concentration changes in the AMB contribute to the pollution plume moving along the S–N valley to the Pyrenees. Our results indicate that O_3 abatement strategies cannot rely only on NO_x emission control but must include a significant reduction in anthropogenic sources of VOCs. In addition, our results show that mitigation strategies intended to reduce O_3 should be designed according to the local meteorology, air transport, particular ozone regimes and AOC of the urban area.

https://doi.org/10.5194/egusphere-2023-160
Preprint. Discussion started: 8 March 2023

1 Introduction

Tropospheric ozone (O_3) is a radiatively active gas that acts as an oxidizing agent and a surface pollutant in urban areas, where it is a major component of photochemical smog and causes a number of respiratory health effects (Sillman, 2003; Anenberg et al., 2010). In 2019, it was estimated that 365,000 respiratory mortalities worldwide were due to anthropogenic O_3, representing an increase of $\sim 16\%$ with respect to 2010 (GBD 2019 Risk Factors Collaborators, 2020). The World Health Organization (WHO) provides guidelines to protect humans from exposure by reducing the levels of key air pollutants, including ozone. The WHO released revised air quality guidelines in 2021, keeping the O_3 levels to 100 μg m-3 for an 8-hour daily average and recommending 60 μg m^{-3} for an 8-hour daily average during the six consecutive months with the highest average ozone concentrations (Organization, 2021).

Ozone is photochemically produced through nonlinear chemical processes, involving mainly reactions of nitrogen oxides (NO_x= NO_2+NO) and volatile organic compounds (VOCs); this results from both anthropogenic and biogenic sources in the presence of sunlight (Monks et al., 2015; Crutzen, 1974; Derwent et al., 1996). This chemistry occurs in two photochemical regimes, NOx-sensitive and VOC-sensitive (Sillman et al., 1990; Sillman, 1999). In the NOx-sensitive regime (low NOx and high VOC), ozone production is controlled (or limited) by the concentration of NO_x, therefore, the O_3 levels increase with increasing NO_x, and there are only small changes with increases in the VOC levels. In this regime, O_3 reacts mainly with hydrogenated species to form hydrogen peroxide (H_2O_2), which is removed by wet and dry deposition. In the VOC-sensitive regime (high NO_x), ozone levels increase with increased VOC concentrations and decrease with increased NO_x concentrations. This last regime is typical of urban areas where a reduction in NO_x emissions enhances ozone levels locally due to the higher levels of oxidants (mainly hydroxyl radicals, OH) and reactions with VOCs. Peak concentrations of ozone usually occur during the midday hours, when the sunlight is most intense. However, during the afternoon and evening, high ozone concentrations are observed in remote areas due to higher biogenic VOC emissions, less titration by NO, and transport of O_3 and its precursors from their sources. At night and next to a source with high emissions of NO (e.g., power plants), ozone is lost through the process of NO_x titration and forms NO_2, which is subsequently converted to nitric acid (HNO_3) and removed from the atmosphere by wet and dry deposition (Monks et al., 2015). In summary, O_3 levels can be reduced only if there are reductions in the amounts of the precursors NO_x, VOC and carbon monoxide (CO). Reductions in VOC emissions would be an effective pathway to reducing ozone in a high NO_x area (VOC-sensitive). On the other hand, reductions in NO_x emissions would be effective in reducing O_3 if NO_x-sensitive chemistry dominates. In urban areas, this photochemistry illustrates the difficulties involved in developing policies to reduce O_3 in polluted regions (Sillman, 2003). Thus, a more profound understanding of the sensitivity of local ozone formation to changes in NO_x and VOC levels is essential for developing effective air quality policies. Other important processes for removal of O_3 are reactions of halogens species (Badia et al., 2021a), which remove 30–35 Tg (11–15 %) of tropospheric ozone, and dry deposition, which accounts for about 20% of the O_3 lost from the troposphere (Wild, 2007).

In addition to photochemical reactions, the concentration of ozone is sensitive to meteorological variables such as solar radiation and wind speed and direction (Neiburger, 1969). Ozone production is intensified on warm, sunny days when the

https://doi.org/10.5194/egusphere-2023-160
Preprint. Discussion started: 8 March 2023

air is stagnant. Therefore, the increase in frequency, severity, and duration of heatwaves during recent decades increases the need to understand the influence of meteorological drivers and anthropogenic factors on ground-level ozone pollution. This is becoming more important for urban cities in the Mediterranean area with high summer temperatures, and heatwaves are projected to become more severe in the future due to anthropogenic climate change (Pyrgou et al., 2018; Zittis et al., 2015).

Indeed, local ozone levels depend not only on local production and loss mechanisms that are sensitive to meteorological factors but also on the transport of ozone and its precursors. Previous studies have shown that ambient ozone concentrations are strongly influenced by transport of regional ozone and its precursors, while local precursor emissions play limited roles in ozone formation (Romero-Alvarez et al., 2022; Kleanthous et al., 2014). Cristofanelli and Bonasoni (2009) showed that the background tropospheric ozone concentration in the Mediterranean area and southern Europe is affected mainly by three transport processes: 1) regional and long-range transport of pollutants, 2) downwards transport from the stratosphere, and 3) transport of dust from the Sahara Desert.

The lockdown period provided a significant reduction in ozone precursors, and it represents an excellent opportunity to further our understanding of the photochemical reactions involved in ozone chemistry. Estimated average emission reductions in Spain during the most severe lockdown period were reported, with road and air traffic reductions reaching 80-90% Guevara et al. (2021). During this period, Guevara et al. (2021) estimated the average emission reductions at the EU-30 level to be -33% for NO_x. Consequently, restrictive mobility measures that included important reductions in traffic had many positive environmental impacts, 70 and improvements in air quality were reported globally (Liu et al., 2020; Venter et al., 2020a; Sharma et al., 2020).

Previous modelling studies analysed the changes in air quality, emissions, and chemical regimes seen on global and regional scales during the COVID-19 lockdown (Miyazaki et al., 2021; von Schneidemesser et al., 2021; Roozitalab et al., 2022; Sicard et al., 2020; Badia et al., 2021). A global modelling study by Miyazaki et al. (2021), showed that the global total tropospheric ozone burden declined by 6 Tg (∼2%) during May-June 2020, mainly due to emission reductions in Asia and the Americas. The modelling study of Venter et al. (2020b) found that, after taking into account the meteorological variations, lockdown measures have reduced the levels of NO_2, mainly due to the reduction in transportation, and PM levels by approximately 60% and 31% in 34 countries, with a general increase in O_3 of 4% (-2 to 10%). Sicard et al. (2020) described ozone increases in cities (17% in Europe, 36% in Wuhan) resulting from lower titration of O_3 by NO due to the strong reduction in NO_x emissions from road transport. Most of this literature was focused only on the lockdown period, and the de-escalation period, which had different ozone chemistry, was not analysed. In addition, these studies did not discuss changes in the chemical regimes arising for different land uses and the transport of pollutants due to lockdown measures from cities to rural areas.

Only a few studies have reported that enhanced atmospheric oxidation capacity (AOC) contributed to O_3 increases during the COVID-19 lockdown due to increases in the major oxidants OH, hydroperoxy radical (HO_2) and nitrate radical (NO_3) (Zhu et al., 2021; Wang et al., 2021b, 2022). The predominant oxidant for AOC during the daytime is OH, which is responsible for the oxidation and removal of most natural and anthropogenic trace gases (Elshorbany et al., 2009; Saiz-Lopez et al., 2017). During the night, the concentration of OH is significantly reduced, and the AOC is then controlled by NO_3, together with O_3, which is also an important oxidant (Elshorbany et al., 2009; Saiz-Lopez et al., 2017). During the lockdown, the significant

https://doi.org/10.5194/egusphere-2023-160
Preprint. Discussion started: 8 March 2023

decreases in NO_2 concentrations increased the OH levels, which led to the formation of harmful oxidants such as O_3 (Zhu et al., 2021; Wang et al., 2021b, 2022).

In recent decades, EU emission mitigation policies have been successful in decreasing emissions of key air pollutants such as SO_2, NO_x, NMVOCs, and PM (Sicard et al., 2021; and European Environment Agency et al., 2019). However, the current levels for the secondary air pollutant O_3 in cities continue to exceed the EU standards and WHO air quality guidelines (Guerreiro et al., 2014; and European Environment Agency et al., 2019). Indeed, local ozone pollution mitigation efforts are generally inefficient, mainly because 1) ozone formation depends on nonlinear chemical interactions, 2) with a lifetime of several weeks, ozone levels are strongly influenced by long-distance transport, which is associated with specific weather conditions and the hemispheric background, and 3) its precursors are emitted mostly far from the sites of ozone exceedances. Sicard et al. (2013) found a decrease in annual O_3 averages (-0.4% yr-1) at rural sites and an increase at urban and suburban stations (0.6% and 0.4%, respectively) during 2000–2010 for the Mediterranean area. These changes resulted from the mitigation policies for NO_x and VOC emissions in the EU that led to an increase in O_3 levels in urban areas due to a reduction in titration by NO. Therefore, there is an urgent need to expand our knowledge of ozone chemistry to help decision-makers choose better mitigation strategies.

In the present study, we use the air quality model WRF-Chem coupled with the urban canopy model BEP-BEM to investigate the response of NO_x-VOCs-O_3 chemistry to changes in precursor emissions in the Metropolitan Area of Barcelona (AMB); this furthers our understanding of ozone formation mechanisms and transport to rural areas, and it enables the design of effective air quality mitigation strategies. We compare the ozone levels for two periods with very different anthropogenic and biogenic activity levels: March and April 2020, when ozone precursors were at their lowest levels because of repeated lockdowns due to COVID, and 2) May 2020, when the AMB was in a de-escalation plan but the ozone levels were typically highest because of the bloom of biogenic emissions under the intense sunlight conditions. In addition, ozone production regimes for different land uses of the AMB are analysed to determine changes in the NOx/VOC ratio in different areas of the city that are affected by different biogeochemical effects (biogenic VOC emissions, dry deposition, anthropogenic emissions of ozone precursors). Here, we also discuss changes in the AOC and propose that the AOC should be considered when designing air quality control policies. Changes in ozone circulation from the AMB to the Pyrenees mountains are also discussed for specific days characterized by high ozone levels.

The case study is described in Sect. 2. The air quality model, including the model setup, validation, and simulations, is described in Sect. 3, followed by the results (Sect. 4). A discussion of the ozone chemistry that includes ozone sensitivity, AOC and transport from the city to rural areas is presented in Sec. 5.

2 Case study

The Metropolitan Area of Barcelona (AMB) serves as our case study. It is located in Catalonia (Spain) in the northeastern part of the Iberian Peninsula (Fig. 1). This region is characterized by a Mediterranean climate, with dry and hot summers and clear skies. Due to a complex orographic territory with different altitudes and several peripheral mountain ranges and depressions, it

https://doi.org/10.5194/egusphere-2023-160
Preprint. Discussion started: 8 March 2023

is not easy to generalize the climatic features of the Catalan lands for the whole territory (Martín-Vide et al., 2010). The AMB, with more than 3 million people, is the most populated urban area on the Mediterranean coast.

The city of Barcelona annually reports some of the highest air pollution levels in Europe, and the most problematic pollutants are NO_2, PM2.5, and PM10 (Rivas et al., 2014). In particular, in 2019, the NO_2 annual mean levels in the high traffic urban air pollution ground monitoring stations (Eixample and Gràcia-Sant Gervasi) exceeded the WHO guideline (40 μg m$^-$3) (Rico et al., 2019). In the same year, the mean values for PM2.5 and PM10 exceeded the WHO guideline (20 and 10 μg m$^-$3, respectively) at all urban stations in the city (Rico et al., 2019). Exceeding these air quality reference levels is associated with significant risks to public health (Organization, 2021; Rivas et al., 2014). The year 2020 was the first year in which the NO_2 values in Barcelona remained within the WHO limits (Rico et al., 2020) due to the significant reduction in traffic emissions that resulted from the Spanish government's emergency rule and its lockdown restrictions (see Supplement Fig. S1). Note that 2020 had more rainfall than previous years, which has important implications for the removal of pollutants from the air.

Another air quality problem was found for the Vic plain (see Fig. 1), which records the highest number of exceedances for hourly O_3 levels (180 μg m$^-$3) when the sea breeze transports the ozone precursors from AMB inland to this rural plane (Querol et al., 2017; Massagué et al., 2019; Jaén et al., 2021). During the late spring and summer seasons, the combination of daily upslope winds and sea breezes may cause the intrusion of polluted air masses up to 160 km inland. Thus, the air massed from a polluted area (such as the AMB) can be transported northwards and injected at high altitudes (2000–3000 masl) by the Pyrenean mountain ranges (Querol et al., 2017; Massagué et al., 2019).

Ozone levels were higher compared to previous years in Ciutadella, the background station in Barcelona, during the period March-June 2020 (see Supplement Fig. S2). In Tona, a rural station located in the Vic Plain and situated 45-70 km north of Barcelona and surrounded by high mountains, and in Pardines, also a rural site situated in the Pyrenees mountains (see Fig. 1), high ozone concentrations were registered and clearly exceeded the WHO limit of 60 μg m$^-$3 for peak seasons. Ozone levels were high in these two rural stations during March-June with higher values for 2015-2019 compared to 2020 due to the reduced emissions in the AMB. Note that for some weeks, the O_3 levels were higher in 2020 than in 2015-2019 due to meteorological conditions that increased the levels of ozone precursors (see Supplemental Figs. S1 and S2).

In this study, we selected two periods to discuss the changes in O_3 chemistry: 1) a full lockdown period (30 March-12 April, weeks 3-4 in Table 1), in which we found the highest mobility reduction and 2) a relaxation period (18-30 May, weeks 10-11 in Table 1), when restrictions started to relax and O_3 formation increased due to the warm temperatures of the late spring (see Table 1).

The first period was characterized by meteorological dynamism in the Iberian Peninsula. The period began with a high-pressure centre in the northern Atlantic Ocean, which generated a cold and dry continental NE flux over Europe. General precipitation was registered in Catalonia during the first days (March 30 – April 4), caused by a low-pressure centre that moved from the Atlantic to the Mediterranean. These conditions were optimal for generating precipitation in the Mediterranean area of the peninsula. The next days were defined by high pressures over Europe, which generated a more stable meteorology with isolated precipitation and a warm air mass crossing Europe from the south. During this period, no important fluxes from any directions were detected. At the surface level, the Azores anticyclone became stronger and reached pressures above 1030 hPa

https://doi.org/10.5194/egusphere-2023-160
Preprint. Discussion started: 8 March 2023

over the Atlantic. The second period had more stability due to a strong anticyclonic ridge covering the SW and centre of Europe, resulting in typical summer weather. Winds from the N and NW were detected NE of Catalonia and in the Ebro Valley, respectively, due to the Pyrenees natural barrier, which modifies the trajectories of superficial winds. Low pressures were found over Italy, which intensified the winds from the north over the east of the peninsula. The last days of this period (May 24–30) registered weak precipitation in the Pyrenees and the area NE of Catalonia, with weak winds from different directions (turning from north to south). This was caused by a strong anticyclone located in northern Europe (over 1030 hPa), which generated an undetermined situation with no effects of high or low pressures in the Peninsula. See Table 1) for a summary of the meteorological conditions for these periods.

In addition, we select two days in the lockdown period (the 3rd and 6th of April) and two days in the relaxation period (the 22nd and 26th of May), during which high ozone concentrations were registered (see Table S1 in the Supplement), to study the changes in the O_3 circulation from Barcelona (Ciutadella) to the Pyrenees mountains (Pardines), including the Vic plane (Tona) and Montseny. The mean surface temperatures, pressures at the surface level and accumulated precipitation among other meteorological variables for these days are presented for the four sites (Ciutadella, Montseny, Tona and Pardines) in Table S2 of the Supplement. According to the meteorological data from the Servei Meteorològic de Catalunya Servei Meteorològic de Catalunya (SMC), there was no precipitation during these four days except in the Pyrenees (2.9 mm) on the 22nd of May, the wind intensity was low and the surface temperatures were significantly high for this time of the year during the two days in May.

To supplement this information, Figures 3 and 4 show the trajectories of the air masses arriving at the monitoring stations on the selected days; which were modelled with the Lagrangian particle dispersion model FLEXPART-WRF (Brioude et al., 2013). This version of the Lagrangian model works with the Weather Research Forecasting (WRF) mesoscale meteorological model, with the same parametrization as the WRF-Chem model (see section 3.1). The transport model has been run in backwards mode, which means that what is represented in each plot is the residence time, at each grid cell of the map, for the air masses arriving at each site. Twenty-four-hour back trajectories were calculated for each day at a release time of 16 h and with a grid cell size of 0.03 $\times$ 0.03 degrees. The air masses on the 3rd of April and 22 of May were transported from the AMB to rural areas such Montseny and the Vic Plain, and we can see an influence from the bottom layers (0-300 m) and the upper layers (300-2000 m) at the different sites. The air masses on the 6th of April were channelled from the AMB northwards to Montseny, the Vic Plain and the Pyrenees. The air masses on the 26th of May were also transported from the AMB northwards to Montseny, the Vic Plain and the Pyrenees, but the air masses that arrived at the surfaces of these locations had strong local components and a larger influences from the upper layers.

3 Air quality model

We used the regional chemistry transport model WRF-Chem (Grell et al., 2005) version 4.1, a highly flexible community model for atmospheric research in which aerosol–radiation–cloud feedback processes are considered. The WRF-Chem model

https://doi.org/10.5194/egusphere-2023-160
Preprint. Discussion started: 8 March 2023

is widely used for simulations of air pollution episodes (Georgiou et al., 2018; Yegorova et al., 2011) and, in particular, the air quality over the AMB has been analysed in Badia et al. (2021).

3.1 Model set-up

The WRF-Chem model is configured with two domains covering the Iberian Peninsula (D1: 9 km×9 km) and the Catalonia region (D2: 3 km×3 km) with 45 vertical layers up to 100 hPa (Fig. 2). The meteorological and chemical initial and lateral boundary conditions (IC/BCs) were determined using the ERA5 global model data (Hersbach et al., 2020) and WACCM (Gettelman et al., 2019), respectively. The HERMESv3 preprocessor tool (Guevara et al., 2019) was used to create the anthropogenic emissions files from the CAMS-REG-APv3.1 database (Granier et al., 2019). This emission inventory is based on data from 2016. Biogenic emissions are computed online from the Model of Emissions of Gases and Aerosols from Nature v2 (MEGAN; Guenther et al. (2012)). For the gas-phase chemical scheme, we used the Regional Acid Deposition Model (RADM2, Stockwell et al. (1990)), which accounts for 63 chemical species, 21 photolytic reactions and 136 gas-phase reactions. NMVOC oxidation in RADM2 only explicitly treats ethane, ethene, and isoprene species, and all other NMVOCs are classified as grouped species based on OH reactivity and molecular weight. Thus, the RADM2 gas-phase chemical mechanism grouped the VOCs into 14 species, such as alkane, alkene, aromatic, and formaldehyde. In WRF-Chem, RADM2 is coupled to the MADE/SORGAM aerosol module (Ackermann et al., 1998; Schell et al., 2001). RADM2 has been broadly used in studies of the air quality over Europe (Im et al., 2015; Tuccella et al., 2011)

Here, we used a multilayer layer urban canopy scheme, the building effect parameterization (BEP) coupled with the building energy model (BEP+BEM, (Salamanca et al., 2011)) to represent the urban areas in our domain; this takes into account the energy consumed by buildings and the anthropogenic heat, which has been previously validated for the area under study (Ribeiro et al., 2021; Segura et al., 2021). The local climate zone (LCZ) classification (Stewart and Oke, 2012) is used for the AMB, which associates specific values of the thermal, radiative and geometric parameters of the buildings and ground into 11 urban classes, which are used by the BEP+BEM urban canopy scheme to compute the heat and momentum fluxes in the urban areas (see Segura et al. (2021) for more details on the use of LCZ and urban morphology). We performed a spin-up of 1 month. Table 2 describes the main configuration of the model.

3.2 Description of the simulation cases

To better understand the impacts of emission reduction measures on air quality, the WRF-Chem model was utilized to calculate the changes in O_3 chemistry during the COVID lockdown period. We ran two simulations: 1) Business As Usual (BAU) and COVID for the period of March-June 2020 (see Table 1). The COVID run used the emissions changes provided by the Barcelona Supercomputing Center (Guevara et al., 2021), which were previously used in other studies (von Schneidemesser et al., 2021; Brancher, 2021). These emission changes varied per day, country and sector. Figure 5 displays the emission changes used in this study, and the highest changes were found for the road transport (up to 80%) and aviation (up to 90%) sectors. Inputs for the other emissions (biogenic, dust, sea-spray) and meteorology used in WRF-Chem were set to be consistent. As

https://doi.org/10.5194/egusphere-2023-160
Preprint. Discussion started: 8 March 2023

a result, the differences in pollutant concentrations calculated by WRF-Chem were attributed to changes in the anthropogenic emissions.

3.3 Model validation

Several meteorological and air quality stations were used herein to evaluate the model (COVID simulation) for the lockdown (30 March to 12 April 2020) and relaxation (18 to 30 May 2020) periods. The same model configuration has been evaluated previously over the AMB for the meteorology (Ribeiro et al., 2021; Segura et al., 2021) and the chemistry, without any reduction in anthropogenic emissions (Badia et al., 2021), for different periods.

3.3.1 Meteorology

The meteorological data used to validate our model were from the Xarxa d'Estacions Meteorològiques Automàtiques (XEMA). Stations within this network are classified as urban and rural according to the land use of the model. Herein, we used data for the wind speed (WS), temperature (T) and relative humidity (RH). Tables S3 and S4 in the Supplement present statistical evaluations of hourly data for the Metropolitan Area of Barcelona (AMB) and Catalonia (CAT) region for the lockdown (30 March to 12 April) and relaxation (18 to 30 May) periods, respectively.

The validations of the WRF-Chem simulation (COVID run) revealed that the model generally reproduced the air temperatures of the two simulation periods well, but the performance was poorer in representing the relative humidity and the wind speed. For the first period, the simulated air temperatures for the urban stations showed low positive biases of 0.4 °C and 0.3 °C for the AMB and CAT, respectively, and an RMSE of 1.4 °C. The rural stations presented a higher bias inside the AMB (0.9 °C), which resulted from erroneous descriptions of the land use at the model resolution level (3 km). Loose performance was found for the relative humidity and the wind speed, with average RMSEs of 12.2% and 2.5 m/s, respectively. The model underestimated the relative humidity in the urban and rural areas of the AMB by 2.0% and 5.2%, respectively, while it overestimated the humidity in the rural areas of the CAT (1.4%). In the case of the wind speed, the model overestimated the wind flow over the entire domain (1.5 m/s on average in CAT), especially in the rural areas of CAT (1.9 m/s). For the second study period, a similar performance was obtained for the air temperatures inside the AMB, with a slight increase in the RMSE (1.5 °C and 1.6 °C for urban and rural areas) and a decrease in the correlations between modelled and observed data (0.90 and 0.92, respectively). Unlike the first period, the model overestimated the relative humidities at all stations in the second period, except for the rural stations in the AMB (-3.8%). The model provided lower overestimates for the wind speeds during the second period (1.0 m/s on average in CAT), although the correlations decreased in the second period.

3.3.2 Air quality

Air quality data from the monitoring stations Xarxa de Vigilància i Previsió de la Contaminació Atmosfèrica (XVPCA) were used here. Stations in this network were classified into different groups: urban background, urban traffic, suburban background, and rural. Here, we used the data for O_3 and NO_2. Tables S5 and S6 in the Supplement present statistical evaluations of

https://doi.org/10.5194/egusphere-2023-160
Preprint. Discussion started: 8 March 2023

hourly data for the AMB and Catalonia during the lockdown (30 March to 12 April) and relaxation (18 to 30 May) periods, respectively. The modelled concentrations were converted to units of μg m$^{-}3$ by using the temperatures and pressures from the model.

Overall, the model (COVID simulation) showed reasonable agreement with the observations for NO_2 and O_3 concentrations during both periods. The best performance in the lockdown period was observed over the urban background (R between 0.43 and 0.45 for NO_2 and between 0.70 and 0.73 for O_3), while low R values were found over the rural areas (0.32 for NO_2 and 0.42 for O_3). The performance for the relaxation period was not as good as that for the lockdown period, with R values between 0.24-0.40 for NO_2 and 0.42-0.62 for O_3. However, there were negative and positive biases in both periods for NO_2 (NMB between -0.15 and -0.66) and O_3 (NMB between 0.13 and 0.28), respectively. Similar biases were seen in another study (von Schneidemesser et al., 2021). Part of our model bias was attributed to the 1) boundary conditions used for this study (WACCM model) that added a bias to the O_3 background levels (Giordano et al., 2015) and 2) the current emission inventory was too coarse to accurately represent the spatial distributions and temporal variations in NO_x emissions, e.g., from road transport. Low values for the modelled NO_x levels underestimated ozone loss via NO titration, which resulted in high nighttime surface ozone concentrations. The lifetime of surface NO_x (few hours) is shorter than that of O_3 (days or weeks); thus, the surface NO_x concentrations are very sensitive to emissions. We should also mention that there might be large uncertainties for the calculations of emissions factors, as discussed in Doumbia et al. (2021); underestimates of traffic NO_x emissions over Europe have been mentioned previously in several air quality modelling studies (von Schneidemesser et al., 2021; Karl et al., 2017).

4 Results

4.1 Air quality changes

In the first period (30 March to 12 April), the results (difference between the COVID and BAU runs) showed a general reduction in NO_2 concentrations all over the Catalonia region at the surface level, with high reductions found during the evening peaks (19-21 UTC) and over the AMB (-2 to -18 μg m^{-3}, -10 to -70%) (see Fig. S3 in the Supplement). The highest reductions were found around the airport due to a significant reduction in air traffic emissions (see Figure 5). The surface concentrations of VOCs were slightly lower during the morning peak (up to -2 μg m^{-3}, -10%) (see Fig. S4 in Supplement). During the evening peak, there were also decreases seen for several areas of the AMB and Catalonia (up to -1.5 μg m^{-3}, -12%). However, we also observed slight increases in some areas (up to 0.1 μg m^{-3}, 1%). Note that during the lockdown, the VOC emissions increased in the stationary combustion sector (see Figure 5). Changes in emissions that showed a significant decreases in NO_2 concentrations and slight decreases in VOC concentrations enhanced O_3 levels over the AMB. This is consistent with the observations (see Figs. S1-S2 in the Supplement). The reduced O_3 production resulting from reductions in the levels of the O_3 precursors was overwhelmed by a reduction in the extent of NO titration, resulting in a net increase in O_3 levels. During the evening peaks (19-21 UTC), we found the highest changes (1 to 18 μg m^{-3}, 1 to 20%). However, when surface O_3 concentrations were higher (afternoon peak, 13-15 UTC), the increases were much lower (up to 6 μg m^{-3}, 6%) than those for the evening peak (see Fig. S5 in Supplement). Outside the AMB, the concentrations did not differ significantly (< 2 μg

https://doi.org/10.5194/egusphere-2023-160
Preprint. Discussion started: 8 March 2023

m^{-3}, < 2%) for the two simulations. Differences in the O_x (NO_2 + O_3) values were calculated to aid our interpretation of the O_3 concentrations by diminishing the effect of O_3 titration by NO in highly polluted areas (see Fig. S6 in Supplement). The overall changes in the O_x concentrations remained practically constant due to a balance between the increases in O_3 levels and decreases in NO_2 levels. This has important policy implications because one air pollutant problem is being replaced by another. A similar result was seen by von Schneidemesser et al. (2021) in their study of Berlin during the lockdown.

The differences between the BAU and COVID simulations for the second period (18 to 30 May) showed overall reductions in the NO_2 (-2 to -15 μg $^{-3}$, -10 to -65%) and VOC levels (up to -2 μg m^{-3}, -16%), with high reductions found during the evening peaks (see Fig. S3 in the Supplement). Ozone levels decreased (by up to 3.5 μg m^{-3}, see Fig. S5 in the Supplement) in most of Catalonia due to significant reductions in most of the emission sectors (see Figure 5) during the COVID simulation, which decreased the high ozone productivity normally seen for this time of the year. However, we still found enhanced O_3 levels around the Barcelona airport in the evenings; the reductions in emission levels were still significant (more than 80%, see Figure 5) and inhibited titration of the O_3 by NO. Note that in this case, the O_x concentrations decreased nearly everywhere in the Catalonia area and up to -4 μg m^{-3} over the AMB (see Fig. S6 in Supplement) for the COVID simulation, resulting in overall improvements in the air quality.

5 Discussion

5.1 O_3 Sensitivity to precursors and land-use

Variations in the levels of the O_3 precursors (NO_x and VOCs) had large effects on O_3 production. We represent this complex relationship in Figures 6 (6:00 to 8:00 UTC), 7 (13:00 to 15:00 UTC), and 8 (19:00 to 21:00 UTC), which show the differences in surface NO_x, VOC, and O_3 concentrations in the BAU and COVID simulations during the first period (30 March to 12 April, only weekdays) and the second period (18 to 30 May, only weekdays). Each dot of the top row corresponds to the O_3 concentration difference (ppb) of one grid cell of the AMB at the surface level. To complement this information, we calculated the average NO_x/VOC ratios for these two periods in Table 3. The dots in the lower row represent the land use for each grid cell, which is the key to understanding how industrial, open urban, compact urban, water, agriculture, natural open and forestland uses influenced the O_3 regimes (see Figure S11 and Table S9 in the Supplement for more detail on the land use classification). Values of NO_x and VOC concentrations and relative changes for each land use are shown in Tables S7 and S8 in the Supplementary Information. In Figure 6-8, we indicate the NOx-limited regime with a dark solid line separating VOC:NO_x >8, which is typical for locations located downwind of urban and suburban areas, and the VOC-limited regime (VOC:NO_x <8) which is typical for highly polluted urban areas (Sillman, 2003). We also indicate the transitional regime with two dotted lines (VOC:NO_x >4/1 and VOC:NO_x <15/1) showing where ozone becomes less sensitive to NO_x changes and increases with increasing VOC levels, as identified in other studies (Wang et al., 2021a; Yang et al., 2021).

Overall, without any reduction in emissions (BAU simulation), this analysis indicates that in green areas, such as urban forests far from anthropogenic sources and influenced by high biogenic VOC emissions, ozone production is NO_x-sensitive in the mornings and afternoons. With the inland sea-breeze fronts seen in the late afternoons/early evenings (Massagué et al.,

https://doi.org/10.5194/egusphere-2023-160
Preprint. Discussion started: 8 March 2023

2019), pollutants are transported from their sources (urban areas) to other areas (green areas). Consequently, we found a transition to a VOC-limited regime in green areas in the evenings. Some of the grids classified as naturally open and agriculture are close to the Barcelona airport (high NO_x sources), and the transport of pollutants (driven by the wind speed and direction) has a significant impact on their regime. However, we see that most of the grids classified as naturally open are NOx-limited all day. In the case of grids classified as agriculture, we see that in the morning and evening, most of these grids are in the transition or VOC-limited regimes, while in the afternoon, these grids are in the transition or NOx-sensitive regimes. Areas close to highly polluted areas (including urban areas such as compact urban, industrial, and water areas) are in VOC-sensitive or transitional regimes all day, especially during the evening due to high traffic emissions. Note that "water points" are located around the harbour and the airport and are typically high NO_x sources. In terms of ozone levels, high values are found during the morning (40-43 ppb) and evening (46-47 ppb) hours in suburban areas (forest and natural open) because there is less NO (because of less traffic) and thus less ozone degradation. In the afternoon, high O_3 levels are found everywhere in the AMB (49-55 ppb), especially over the urban areas (industrial, open urban and compact urban).

With the significant decrease in NO_x (20-40%) and a slight decrease in VOC (1-5%) levels during the lockdown, the O_3 levels increased for the COVID run (1-5%), and chemical formation tends to enter the NOx-sensitive regime, especially in the morning and afternoon hours during April-March. In the case of green areas (forest, natural open and agriculture), we see clear transitions towards NOx-sensitivity regime. However, despite the cuts in emissions, most of the grids close to highly polluted areas (compact urban, industrial, and water) were still in the VOC-sensitive or transitional regimes all day, especially in the evenings (high traffic emissions), for which we found the highest ozone increases (2.4-5%). Similar results were found when we compared both runs (BAU and COVID) for the period in May in terms of the changes in the chemical for each land use. However, we found that during May, the maximum ozone levels decreased in the COVID run during the afternoons (up to 1.6% in green areas), which was attributed to reductions in the anthropogenic emissions that decreased the ozone precursor levels (24 to 40% for NO_x and 24 to 40% for VOCs) and consequently ozone production. For green areas far from anthropogenic sources (forests), the ozone levels were also reduced in the mornings and evenings during this period.

The lockdown measures inhibited NO titration of the O_3, mainly due to changes in the local NO_x emissions resulting from road transport. This resulted in an increase in the O_3 levels during the evening hours, where there was no photolytic reaction with NO_2, in urban areas with high population densities. We found that air quality policies based solely on transport reduction (as illustrated by the COVID lockdowns, which reduced NO_x levels) actually intensified O_3 levels over urban areas, indicating the need for a protocol with strident control measures to reduce NO_x emissions without significantly reducing anthropogenic VOCs to control O_3 levels. However, high ozone production during May was reduced due to reduced levels of the precursors, and consequently, there were reductions in the maximum ozone levels for that period.

5.2 Impacts on the atmospheric oxidation capacity

In addition to understanding changes in the levels of O_3 precursors, it is important to determine how emission changes affect the atmospheric oxidation capacity (AOC) because this plays an important role in the loss and production rates of primary and secondary pollutants. We saw increases in the concentrations of the oxidants OH and NO_3 during the period March-April,

https://doi.org/10.5194/egusphere-2023-160
Preprint. Discussion started: 8 March 2023

mainly over the AMB, as shown in figures 9 and 10, where the left-hand panels indicate absolute concentrations (COVID-BAU) and the right-hand panels indicate relative changes in comparison to the BAU simulations ((COVID-BAU)/BAU×100). OH is the dominant tropospheric daytime oxidant, and it increases considerably (up to 0.12 ppt, +45%) because of significant reductions in NO_2 levels, since NO_2 is the primary OH sink (Elshorbany et al., 2009). The rises in these free radical levels could be the leading cause for the diurnal O_3 increases given their strong link with O_3 production (VOC and CO oxidation by OH are the initial reactions for ozone formation). In addition, the NO_3 radical, which is a primary night-time oxidant, also increases in areas close to the airport and harbour (4 ppt, 210%). This increase can be explained by reductions in the VOC and NO_2 levels, which are important sinks for NO_3 radicals (Elshorbany et al., 2009; Saiz-Lopez et al., 2017).

During the period in May, we also found increases in the AOC (and O_3), mainly for areas close to the airport and harbour, where there were still important decreases in NO_x emissions. In these areas, OH levels increase up to 0.3 ppt (55%) in the afternoon, and NO_3 increases up to 4 ppt (230%) in the evening. However, other areas showed general decreases in AOC (-0.1 ppt for OH and -2 ppt for NO_3), resulting in decreases in the O_3 levels. Note that for both periods, the decrease in shipping emissions (a source of NO_x) led to increases in the levels of both radicals along the ship tracks.

Our results indicate that changes in the anthropogenic emissions lead to significant changes in the OH and NO_3 radical budgets, which in the case of emission reduction, such as that experienced during the COVID lockdown, lead to enhanced oxidation efficiency in the urban atmosphere of the AMB and O_3 enhancements. However, during the period when O_3 formation increased (May), there was a decrease in the AOC and O_3 levels (except in the airport and harbour areas) during the COVID run. The elevations of O_3 and AOC levels occurred because these areas were still VOC-limited regimes during this period. In terms of air quality policy, it is important to consider the budgets of free radicals so that mitigation strategies are not counterproductive.

5.3 Pollution transport from urban to rural

In addition to studying the mechanisms for ozone formation in the AMB, we also explored how ozone is transported to rural areas to determine the influence of urban pollution. Rural areas far from the city, such as the Vic Plain and the Pyrenees mountain range, are frequently affected by the atmospheric plume transported northwards from the AMB (Massagué et al., 2019). Indeed, ozone exceedances over these places occur when there are high levels of NO_2 (mainly due to road traffic) over the AMB (see section 2). The urban plume is driven inland by southeast and southern combined sea-valley-mountain breeze winds, channelled by north–south valleys, and crosses the coastal and precoastal Catalan Ranges to an intramountain plain. To understand how emission reductions in the AMB can affect the ozone levels in these rural areas, we analysed the differences in ozone concentrations between the COVID and BAU runs for four specific days during which the air masses flowed from the AMB northwards to the Pyrenees (as shown in Figures 3 and 4) and generated high levels of O_3 pollution in the rural areas (see Table S1 and Figures S7-S10 in the Supplement): on April 3rd and 6th there was no precipitation, with slightly high temperatures and low to moderate wind intensity, and on the 22nd and 26th of May there was warm, sunny weather and anticyclonic conditions (see section 2).

https://doi.org/10.5194/egusphere-2023-160
Preprint. Discussion started: 8 March 2023

On the 3rd of April, we found significant differences between the COVID and BAU runs during the afternoon and especially in the evening, when O_3 differences increased up to 2-3 ppb and higher enhancements were found over the Vic Plain (from the surface up to 2000 m), as shown in Figure 11. High ground-level ozone concentrations over the Vic Plain could have been affected by vertical recirculation of the air mass with O_3 reservoirs from the upper layers (see Fig. S7 in the Supplement) to the lower troposphere (Querol et al., 2017; Massagué et al., 2019). Later at night, ozone accumulated on the surface following a decrease in the PBL height (PBLH), and it was removed by deposition and titration. However, the reduction in daytime NO_x emissions in the COVID simulations resulted in less titration capacity and consequently an increase in the ozone levels (1-2 ppb) that remained at the surface layer along the different sites on the S–N trajectory connecting the AMB, Vic and the Pyrenees. For the 6th of April, differences between the COVID and BAU runs were only found during the evenings and later in the nights, and the ozone levels increased in the COVID run (up to 2 ppb at the surface level) from the city of Barcelona to the mountain area of Montseny (Fig. 12). On that day, this increase was not seen for the sites located farther north. Note that ozone decreases (1-2 ppb) were seen in the free troposphere, especially at night.

We found significant decreases in ozone levels in the COVID simulation (up to 3 ppb, from the surface up to 2000 m) from the AMB north to the mountain area of Montseny on both days in May (22nd and 26th), especially during the afternoons when the PBLH was the highest and solar radiation led to enhancement of the sea breeze front, which provided favourable conditions for regional transport (Massagué et al., 2019). The decreases in ozone precursor emissions (COVID simulation) resulted in less ozone production, and consequently, the ozone concentrations decreased (discussed in sections 5.1 and 5.2). This decrease was also seen for the evening hours. Note that at night, when ozone accumulated on the surface following the decrease in the PBLH, there was a slight increase in its levels due to limited titration by NO. However, there were still reductions in the ozone levels from 500 m to 2000 m at night.

Our results showed that reduced ozone precursor levels increased the ozone levels during the evenings and nights in the COVID run due to reductions in the ozone titration process during the period of April-March, not only in urban areas but also in rural areas such as Montseny, Vic Plain, and the Pyrenees. During May, the emissions reductions in the COVID simulation decreased the ozone maximum levels (in comparison with the BAU run) in the afternoon from the city of Barcelona to the mountain areas of Montseny, the Vic Plain, and the Pyrenees, thereby improving the air quality in all these areas. A comparison of these two periods, April-March and May, showed that the mitigation strategies designed to reduce the high ozone levels were more efficient in May, when ozone formation was high (high biogenic emissions coinciding with anticyclonic conditions). Thus, given the importance of meteorology in air pollution events occurring over urban and rural areas, new mitigation strategies are needed to improve the air quality and would result in significant O_3 reductions; the local O_3 coming from the AMB plume would be reduced, as would the recirculated O_3 and thus the intensity of surface O_3 fumigation from high O_3 reservoir layers in other areas.

https://doi.org/10.5194/egusphere-2023-160
Preprint. Discussion started: 8 March 2023

6 Conclusions

Improving air quality is a top priority in urban areas and requires a better understanding of how the O_3 levels respond to changes in the emission levels of the precursors, as well as the ozone formation regimes and the atmospheric oxidation capacity and associated O_3 formation. Furthermore, urban emissions affect the O_3 levels in rural areas outside the cities. In this study, we used the air quality model WRF-Chem to analyse the air quality changes occurring over the Metropolitan Area of Barcelona and other rural areas affected by transport of the atmospheric plume from the AMB during mobility restrictions.

The large reduction in NO_x levels (up to 60%) seen during the lockdown period combined with a slight change in VOC levels (up to 10%) led to increased O_3 concentrations (up to 20% in the evening). The significant increase found in the evening was mainly due to reduced O_3 titration by NO, which prevailed over the lower O_3 production level caused by decreases in the levels of the O_3 precursors. The lockdown occurred during April-March when ozone photochemical production was still not at the highest level. In addition, our results showed a significant increase in the atmospheric oxidation capacity (AOC) indicated by the enhanced oxidant (OH and NO_3) levels, which was consistent with the slight increases seen in the maximum O_3 concentrations during the lockdown. We also found that for several days, these increases were seen further north in rural areas such as the Vic Plain, which produced the most annual exceedances in Spain. Large enhancements over these areas were the result of 1) a higher regional O_3 background level, 2) vertical recirculation of the air masses that transport high concentrations of O_3 from the upper levels to the lower levels, and 3) the contributions of the AMB pollution plume travelling along the S–N valley connecting the AMB and the Vic Plain and the Pyrenees. High ozone levels seriously affect human health and the environment. In addition, the consistent differences seen in O_x (NO_2 + O_3) concentrations during the period April-March have important policy implications, i.e., that effective mitigation strategies designed to reduce air pollutants and their health effects should include reductions in both O_x and VOC levels to avoid increases in ozone levels.

During a period in May exhibiting high ozone production (high biogenic emissions and intense sunlight), decreases in the levels of the ozone precursors NO_2 and VOCs consequently decreased the maximum ozone (up to 4 μg m^{-3}) and O_x (up to 4 μg m^{-3}) concentrations seen over Catalonia. This was consistent with the unchanged or decreased AOCs. For several days, this decrease in the ozone level was seen further north in the rural areas. In this period, we also found ozone enhancements in the evening, mainly due to reduced O_3 titration by NO.

Furthermore, this analysis suggests that there was a tendency for both periods to move towards a NOx-sensitive regime. However, some areas (open urban, compact urban, industrial, water) were still under VOC-limited or transition regimes despite the remarkable NO_x reduction.

We propose that measures intended to reduce ozone precursor emissions (NO_x and VOC emissions) while maintaining stable O_3 formation levels in the AMB would result in important reductions in O_3 levels in both urban and rural areas, especially in the spring-summer when the ozone productivity is the highest. The current policies based on reducing transportation-related emissions alone could unintentionally increase the AOCs in and around large cities, thereby increasing the ozone levels. We also find that air quality policies must be designed in accordance with the VOC/NO_x ratio, which dictate the O_3 sensitivity particular to that city. Furthermore, the significant effect of NO titration demonstrates the importance of defining mitigation

https://doi.org/10.5194/egusphere-2023-160
Preprint. Discussion started: 8 March 2023

strategies focused on VOC reductions. We also propose that more measurements of VOC levels are required to constrain the models representing these chemical processes, given the complexity of the relationship between these pollutants.

Code availability. The WRF-Chem model code is available from http://www2.mmm.ucar.edu/wrf/users/download/get_sources.html (last access: 2 June 2022), with the specific code used in this study available from the authors upon request (alba.badia@uab.cat).

Data availability. Specific data used in this study available from the authors upon request (alba.badia@uab.cat).

Author contributions. AB carried out all the model simulations and data analysis, and led the interpretation of the results and prepared the manuscript with contributions from all co-authors. GV contributed to the interpretation of the results and provided extensive comments on manuscript. RC run the Flexpart model and analysed the output. SV analise the synoptic situation of the domain. VV and RS validate the meteorology of the model with observations.

Competing interests. The authors declare that they have no conflict of interest.

Acknowledgements. This work has been made possible thanks to the financial support of the European Research Council (ERC) Consolidator project: Integrated System Analysis of Urban Vegetation and Agriculture (818002-URBAG), the Spanish Ministry of Science, Innovation and Universities, through the "Maria de Maeztu" programme for Units of Excellence (CEX2019-000940-M), and the funding and recognition awarded to the research group Sostenipra (2021 SGR 00734) by the Department of Research and Universities of the Generalitat de Catalunya. The authors thankfully acknowledge the computer resources at PICASSO and the technical support provided by the Universidad de Málaga (RES-AECT-2020-2-0004). The authors further wish to thank XVPCA for the provision of measurement stations. Also, thanks to the free use of $HERMESv3_GR$ and the developing team for their support. We also thank the Copernicus Global and Regional emissions service for the emission inventory. All the numerical analysis were performed with the HTCondor cluster hosted by the Port d'Informació Científica (PIC). The authors also thank Qinyi Li and Xavier Querol their constructive suggestions and feedback during this study.

https://doi.org/10.5194/egusphere-2023-160
Preprint. Discussion started: 8 March 2023

References

Ackermann, I. J., Hass, H., Memmesheimer, M., Ebel, A., Binkowski, F. S., and Shankar, U.: Modal aerosol dynamics model for Europe: development and first applications, Atmospheric Environment, 32, 2981–2999, https://doi.org/https://doi.org/10.1016/S1352-2310(98)00006-5, 1998.

and European Environment Agency, Guerreiro, C., Colette, A., Leeuw, F., and González Ortiz, A.: Air quality in Europe : 2018 report, Publications Office, https://doi.org/doi/10.2800/777411, 2019.

Anenberg, S. C., Horowitz, L. W., Tong, D. Q., and West, J. J.: An estimate of the global burden of anthropogenic ozone and fine particulate matter on premature human mortality using atmospheric modeling, Environmental health perspectives, 118, 1189–1195, https://doi.org/10.1289/ehp.0901220, 2010.

Badia, A., Langemeyer, J., Codina, X., Gilabert, J., Guilera, N., Vidal, V., Segura, R., Vives, M., and Villalba, G.: A take-home message from COVID-19 on urban air pollution reduction through mobility limitations and teleworking, npj Urban Sustainability, 1, https://doi.org/10.1038/s42949-021-00037-7, 2021.

Bougeault, P. and Lacarrere, P.: Parameterization of Orography-Induced Turbulence in a Mesobeta–Scale Model, Monthly Weather Review, 117, 1872 – 1890, https://doi.org/10.1175/1520-0493(1989)117<1872:POOITI>2.0.CO;2, 1989.

Brancher, M.: Increased ozone pollution alongside reduced nitrogen dioxide concentrations during Vienna's first COVID-19 lockdown: Significance for air quality management, Environmental Pollution, 284, 117 153, https://doi.org/https://doi.org/10.1016/j.envpol.2021.117153, 2021.

Brioude, J., Arnold, D., Stohl, A., Cassiani, M., Morton, D., Seibert, P., Angevine, W., Evan, S., Dingwell, A., Fast, J. D., Easter, R. C., Pisso, I., Burkhart, J., and Wotawa, G.: The Lagrangian particle dispersion model FLEXPART-WRF version 3.1, Geoscientific Model Development, 6, 1889–1904, https://doi.org/10.5194/gmd-6-1889-2013, 2013.

Cristofanelli, P. and Bonasoni, P.: Background ozone in the southern Europe and Mediterranean area: Influence of the transport processes, Environmental Pollution, 157, 1399–1406, https://doi.org/https://doi.org/10.1016/j.envpol.2008.09.017, special Issue Section: Ozone and Mediterranean Ecology: Plants, People, Problems, 2009.

Crutzen, P. J.: Photochemical reactions initiated by and influencing ozone in unpolluted tropospheric air, Tellus, 26, 47–57, https://doi.org/10.1111/j.2153-3490.1974.tb01951.x, 1974.

Derwent, R., Jenkin, M., and Saunders, S.: Photochemical ozone creation potentials for a large number of reactive hydrocarbons under European conditions, Atmospheric Environment, 30, 181 – 199, https://doi.org/https://doi.org/10.1016/1352-2310(95)00303-G, 1996.

Doumbia, T., Granier, C., Elguindi, N., Bouarar, I., Darras, S., Brasseur, G., Gaubert, B., Liu, Y., Shi, X., Stavrakou, T., Tilmes, S., Lacey, F., Deroubaix, A., and Wang, T.: Changes in global air pollutant emissions during the COVID-19 pandemic: a dataset for atmospheric modeling, Earth System Science Data, 13, 4191–4206, https://doi.org/10.5194/essd-13-4191-2021, 2021.

Elshorbany, Y. F., Kurtenbach, R., Wiesen, P., Lissi, E., Rubio, M., Villena, G., Gramsch, E., Rickard, A. R., Pilling, M. J., and Kleffmann, J.: Oxidation capacity of the city air of Santiago, Chile, Atmospheric Chemistry and Physics, 9, 2257–2273, https://doi.org/10.5194/acp-9-2257-2009, 2009.

GBD 2019 Risk Factors Collaborators: Global burden of 87 risk factors in 204 countries and territories, 1990-2019: a systematic analysis for the Global Burden of Disease Study 2019, Lancet, 396, 1223–1249, 2020.

https://doi.org/10.5194/egusphere-2023-160
Preprint. Discussion started: 8 March 2023

Georgiou, G. K., Christoudias, T., Proestos, Y., Kushta, J., Hadjinicolaou, P., and Lelieveld, J.: Air quality modelling in the summer over the eastern Mediterranean using WRF-Chem: chemistry and aerosol mechanism intercomparison, Atmospheric Chemistry and Physics, 18, 1555–1571, https://doi.org/10.5194/acp-18-1555-2018, 2018.

Gettelman, A., Mills, M. J., Kinnison, D. E., Garcia, R. R., Smith, A. K., Marsh, D. R., Tilmes, S., Vitt, F., Bardeen, C. G., McInerny, J., Liu, H.-L., Solomon, S. C., Polvani, L. M., Emmons, L. K., Lamarque, J.-F., Richter, J. H., Glanville, A. S., Bacmeister, J. T., Phillips, A. S., Neale, R. B., Simpson, I. R., DuVivier, A. K., Hodzic, A., and Randel, W. J.: The Whole Atmosphere Community Climate Model Version 6 (WACCM6), Journal of Geophysical Research: Atmospheres, 124, 12 380–12 403, https://doi.org/https://doi.org/10.1029/2019JD030943, 2019.

Giordano, L., Brunner, D., Flemming, J., Hogrefe, C., Im, U., Bianconi, R., Badia, A., Balzarini, A., Baró, R., Chemel, C., Curci, G., Forkel, R., Jiménez-Guerrero, P., Hirtl, M., Hodzic, A., Honzak, L., Jorba, O., Knote, C., Kuenen, J., Makar, P., Manders-Groot, A., Neal, L., Pérez, J., Pirovano, G., Pouliot, G., San José, R., Savage, N., Schröder, W., Sokhi, R., Syrakov, D., Torian, A., Tuccella, P., Werhahn, J., Wolke, R., Yahya, K., Žabkar, R., Zhang, Y., and Galmarini, S.: Assessment of the MACC reanalysis and its influence as chemical boundary conditions for regional air quality modeling in AQMEII-2, Atmospheric Environment, 115, 371–388, https://doi.org/https://doi.org/10.1016/j.atmosenv.2015.02.034, 2015.

Granier, C., Darras, S., Denier van der Gon, H., Doubalova, J., Elguindi, N., Galle, B., Gauss, M., Guevara, M., Jalkanen, J.-P., Kuenen, J., Liousse, C., Quack, B., Simpson, D., and Sindelarova, K.: The Copernicus Atmosphere Monitoring Service global and regional emissions (April 2019 version), https://doi.org/10.24380/D0BN-KX16, 2019.

Grell, G. A. and Dévényi, D.: A generalized approach to parameterizing convection combining ensemble and data assimilation techniques, Geophysical Research Letters, 29, 38–1–38–4, https://doi.org/https://doi.org/10.1029/2002GL015311, 2002.

Grell, G. A., Peckham, S. E., Schmitz, R., McKeen, S. A., Frost, G., Skamarock, W. C., and Eder, B.: Fully coupled "online" chemistry within the WRF model, Atmospheric Environment, 39, 6957–6975, https://doi.org/https://doi.org/10.1016/j.atmosenv.2005.04.027, 2005.

Guenther, A. B., Jiang, X., Heald, C. L., Sakulyanontvittaya, T., Duhl, T., Emmons, L. K., and Wang, X.: The Model of Emissions of Gases and Aerosols from Nature version 2.1 (MEGAN2.1): an extended and updated framework for modeling biogenic emissions, Geoscientific Model Development, 5, 1471–1492, https://doi.org/10.5194/gmd-5-1471-2012, 2012.

Guerreiro, C. B., Foltescu, V., and de Leeuw, F.: Air quality status and trends in Europe, Atmospheric Environment, 98, 376–384, https://doi.org/https://doi.org/10.1016/j.atmosenv.2014.09.017, 2014.

Guevara, M., Tena, C., Porquet, M., Jorba, O., and Pérez García-Pando, C.: HERMESv3, a stand-alone multi-scale atmospheric emission modelling framework – Part 1: global and regional module, Geoscientific Model Development, 12, 1885–1907, https://doi.org/10.5194/gmd-12-1885-2019, 2019.

Guevara, M., Jorba, O., Soret, A., Petetin, H., Bowdalo, D., Serradell, K., Tena, C., Denier van der Gon, H., Kuenen, J., Peuch, V.-H., and Pérez García-Pando, C.: Time-resolved emission reductions for atmospheric chemistry modelling in Europe during the COVID-19 lockdowns, Atmospheric Chemistry and Physics, 21, 773–797, https://doi.org/10.5194/acp-21-773-2021, 2021.

Hersbach, H., Bell, B., Berrisford, P., Hirahara, S., Horányi, A., Muñoz-Sabater, J., Nicolas, J., Peubey, C., Radu, R., Schepers, D., Simmons, A., Soci, C., Abdalla, S., Abellan, X., Balsamo, G., Bechtold, P., Biavati, G., Bidlot, J., Bonavita, M., De Chiara, G., Dahlgren, P., Dee, D., Diamantakis, M., Dragani, R., Flemming, J., Forbes, R., Fuentes, M., Geer, A., Haimberger, L., Healy, S., Hogan, R. J., Hólm, E., Janisková, M., Keeley, S., Laloyaux, P., Lopez, P., Lupu, C., Radnoti, G., de Rosnay, P., Rozum, I., Vamborg, F., Villaume, S., and Thépaut, J.-N.: The ERA5 global reanalysis, Quarterly Journal of the Royal Meteorological Society, 146, 1999–2049, https://doi.org/https://doi.org/10.1002/qj.3803, 2020.

https://doi.org/10.5194/egusphere-2023-160
Preprint. Discussion started: 8 March 2023

Im, U., Bianconi, R., Solazzo, E., Kioutsioukis, I., Badia, A., Balzarini, A., Baró, R., Bellasio, R., Brunner, D., Chemel, C., Curci, G., Denier van der Gon, H., Flemming, J., Forkel, R., Giordano, L., Jiménez-Guerrero, P., Hirtl, M., Hodzic, A., Honzak, L., Jorba, O., Knote, C., Makar, P. A., Manders-Groot, A., Neal, L., Pérez, J. L., Pirovano, G., Pouliot, G., San Jose, R., Savage, N., Schroder, W., Sokhi, R. S., Syrakov, D., Torian, A., Tuccella, P., Wang, K., Werhahn, J., Wolke, R., Zabkar, R., Zhang, Y., Zhang, J., Hogrefe, C., and Galmarini, S.: Evaluation of operational online-coupled regional air quality models over Europe and North America in the context of AQMEII phase 2. Part II: Particulate matter, Atmospheric Environment, 115, 421–441, https://doi.org/https://doi.org/10.1016/j.atmosenv.2014.08.072, 2015.

Jaén, C., Udina, M., and Bech, J.: Analysis of two heat wave driven ozone episodes in Barcelona and surrounding region: Meteorological and photochemical modeling, Atmospheric Environment, 246, 118 037, https://doi.org/https://doi.org/10.1016/j.atmosenv.2020.118037, 2021.

Karl, T., Graus, M., Striednig, M., Lamprecht, C., Hammerle, A., Wohlfahrt, G., Held, A., von der Heyden, L., Deventer, M. J., Krismer, A., Haun, C., Feichter, R., and Lee, J.: Urban eddy covariance measurements reveal significant missing NOx emissions in Central Europe, Sci. Rep., 7, 2536, 2017.

Kleanthous, S., Vrekoussis, M., Mihalopoulos, N., Kalabokas, P., and Lelieveld, J.: On the temporal and spatial variation of ozone in Cyprus, Science of The Total Environment, 476-477, 677–687, https://doi.org/10.1016/j.scitotenv.2013.12.101, 2014.

Liu, F., Page, A., Strode, S. A., Yoshida, Y., Choi, S., Zheng, B., Lamsal, L. N., Li, C., Krotkov, N. A., Eskes, H., van der A, R., Veefkind, P., Levelt, P. F., Hauser, O. P., and Joiner, J.: Abrupt decline in tropospheric nitrogen dioxide over China after the outbreak of COVID-19, Science Advances, 6, eabc2992, https://doi.org/10.1126/sciadv.abc2992, 2020.

Martín-Vide, J., Brunet, M., Prohom, M., and Rius, A.: Segon informe sobre el canvi climàtic a Catalunya. Capítol 2. Els climes de Catalunya. Present i tendències recents, Tech. rep., Generalitat de Catalunya, 2010.

Massagué, J., Carnerero, C., Escudero, M., Baldasano, J. M., Alastuey, A., and Querol, X.: 2005–2017 ozone trends and potential benefits of local measures as deduced from air quality measurements in the north of the Barcelona metropolitan area, Atmospheric Chemistry and Physics, 19, 7445–7465, https://doi.org/10.5194/acp-19-7445-2019, 2019.

Miyazaki, K., Bowman, K., Sekiya, T., Takigawa, M., Neu, J. L., Sudo, K., Osterman, G., and Eskes, H.: Global tropospheric ozone responses to reduced NO_x emissions linked to the COVID-19 worldwide lockdowns, Science Advances, 7, eabf7460, https://doi.org/10.1126/sciadv.abf7460, 2021.

Monks, P. S., Archibald, A. T., Colette, A., Cooper, O., Coyle, M., Derwent, R., Fowler, D., Granier, C., Law, K. S., Mills, G. E., Stevenson, D. S., Tarasova, O., Thouret, V., von Schneidemesser, E., Sommariva, R., Wild, O., and Williams, M. L.: Tropospheric ozone and its precursors from the urban to the global scale from air quality to short-lived climate forcer, Atmospheric Chemistry and Physics, 15, 8889–8973, https://doi.org/10.5194/acp-15-8889-2015, 2015.

Neiburger, M.: the role of meteorology in the study and control of air pollution, Bulletin of the American Meteorological Society, 50, 957 – 966, https://doi.org/10.1175/1520-0477-50.12.957, 1969.

Organization, W. H.: WHO global air quality guidelines: particulate matter (PM2.5 and PM10), ozone, nitrogen dioxide, sulfur dioxide and carbon monoxide, Tech. rep., World Health Organization, 2021.

Pyrgou, A., Hadjinicolaou, P., and Santamouris, M.: Enhanced near-surface ozone under heatwave conditions in a Mediterranean island, Scientific Reports, 8, https://doi.org/10.1038/s41598-018-27590-z, 2018.

Querol, X., Gangoiti, G., Mantilla, E., Alastuey, A., Minguillón, M. C., Amato, F., Reche, C., Viana, M., Moreno, T., Karanasiou, A., Rivas, I., Pérez, N., Ripoll, A., Brines, M., Ealo, M., Pandolfi, M., Lee, H.-K., Eun, H.-R., Park, Y.-H., Escudero, M., Beddows, D., Harrison, R. M., Bertrand, A., Marchand, N., Lyasota, A., Codina, B., Olid, M., Udina, M., Jiménez-Esteve, B., Soler, M. R., Alonso, L.,

https://doi.org/10.5194/egusphere-2023-160
Preprint. Discussion started: 8 March 2023

Millán, M., and Ahn, K.-H.: Phenomenology of high-ozone episodes in NE Spain, Atmospheric Chemistry and Physics, 17, 2817–2838, https://doi.org/10.5194/acp-17-2817-2017, 2017.

Ribeiro, I., Martilli, A., Falls, M., Zonato, A., and Villalba, G.: Highly resolved WRF-BEP/BEM simulations over Barcelona urban area with LCZ, Atmospheric Research, 248, 105 220, https://doi.org/https://doi.org/10.1016/j.atmosres.2020.105220, 2021.

Rico, M., Font, L., Arimon, J., Marí, M., Gómez, A., and E., R.: Informe qualitat de l'aire de Barcelona, Tech. rep., Agència de Salut Pública de Barcelona, 2019.

Rico, M., Font, L., Arimon, J., Gómez, A., and E., R.: Informe qualitat de l'aire de Barcelona, Tech. rep., Agència de Salut Pública de Barcelona, 2020.

Rivas, I., Viana, M., Moreno, T., Pandolfi, M., Amato, F., Reche, C., Bouso, L., Àlvarez Pedrerol, M., Alastuey, A., Sunyer, J., and Querol, X.: Child exposure to indoor and outdoor air pollutants in schools in Barcelona, Spain, Environment International, 69, 200–212, https://doi.org/https://doi.org/10.1016/j.envint.2014.04.009, 2014.

Romero-Alvarez, J., Lupaşcu, A., Lowe, D., Badia, A., Archer-Nicholls, S., Dorling, S., Reeves, C. E., and Butler, T.: Sources of surface O_3 in the UK: tagging O_3 within WRF-Chem, Atmospheric Chemistry and Physics, 22, 13 797–13 815, https://doi.org/10.5194/acp-22-13797-2022, 2022.

Roozitalab, B., Carmichael, G. R., Guttikunda, S. K., and Abdi-Oskouei, M.: Elucidating the impacts of COVID-19 lockdown on air quality and ozone chemical characteristics in India, Environ. Sci.: Atmos., 2, 1183–1207, https://doi.org/10.1039/D2EA00023G, 2022.

Saiz-Lopez, A., Borge, R., Notario, A., Adame, J. A., de la Paz, D., Querol, X., Artíñano, B., Gómez-Moreno, F. J., and Cuevas, C. A.: Unexpected increase in the oxidation capacity of the urban atmosphere of Madrid, Spain, Scientific Reports, 7, https://doi.org/10.1038/srep45956, 2017.

Salamanca, F., Martilli, A., Tewari, M., and Chen, F.: A Study of the Urban Boundary Layer Using Different Urban Parameterizations and High-Resolution Urban Canopy Parameters with WRF, Journal of Applied Meteorology and Climatology, 50, 1107–1128, https://doi.org/10.1175/2010jamc2538.1, 2011.

Schell, B., Ackermann, I. J., Hass, H., Binkowski, F. S., and Ebel, A.: Modeling the formation of secondary organic aerosol within a comprehensive air quality model system, Journal of Geophysical Research: Atmospheres, 106, 28 275–28 293, https://doi.org/https://doi.org/10.1029/2001JD000384, 2001.

Segura, R., Badia, A., Ventura, S., Gilabert, J., Martilli, A., and Villalba, G.: Sensitivity study of PBL schemes and soil initialization using the WRF-BEP-BEM model over a Mediterranean coastal city, Urban Climate, 39, 100 982, https://doi.org/https://doi.org/10.1016/j.uclim.2021.100982, 2021.

Servei Meteorològic de Catalunya (SMC), .: Butlletí climàtic mensual (maig del 2020), Tech. rep., Departament de Territori i Sostenibilitat., 2020.

Sharma, S., Zhang, M., Anshika, Gao, J., Zhang, H., and Kota, S. H.: Effect of restricted emissions during COVID-19 on air quality in India, Science of The Total Environment, 728, 138 878, https://doi.org/10.1016/j.scitotenv.2020.138878, 2020.

Sicard, P., De Marco, A., Troussier, F., Renou, C., Vas, N., and Paoletti, E.: Decrease in surface ozone concentrations at Mediterranean remote sites and increase in the cities, Atmospheric Environment, 79, 705–715, https://doi.org/https://doi.org/10.1016/j.atmosenv.2013.07.042, 2013.

Sicard, P., Marco, A. D., Agathokleous, E., Feng, Z., Xu, X., Paoletti, E., Rodriguez, J. J. D., and Calatayud, V.: Amplified ozone pollution in cities during the COVID-19 lockdown, Science of The Total Environment, 735, 139 542, https://doi.org/10.1016/j.scitotenv.2020.139542, 2020.

https://doi.org/10.5194/egusphere-2023-160
Preprint. Discussion started: 8 March 2023

Sicard, P., Agathokleous, E., Marco, A. D., Paoletti, E., and Calatayud, V.: Urban population exposure to air pollution in Europe over the last decades, Environmental Sciences Europe, 33, https://doi.org/10.1186/s12302-020-00450-2, 2021.

Sillman, S.: The relation between ozone, NOx and hydrocarbons in urban and polluted rural environments, Atmospheric Environment, 33, 1821–1845, https://doi.org/https://doi.org/10.1016/S1352-2310(98)00345-8, 1999.

Sillman, S.: 9.11 - Tropospheric Ozone and Photochemical Smog, in: Treatise on Geochemistry, edited by Holland, H. D. and Turekian, K. K., pp. 407 – 431, Pergamon, Oxford, https://doi.org/https://doi.org/10.1016/B0-08-043751-6/09053-8, 2003.

Sillman, S., Logan, J. A., and Wofsy, S. C.: The sensitivity of ozone to nitrogen oxides and hydrocarbons in regional ozone episodes, Journal of Geophysical Research: Atmospheres, 95, 1837–1851, https://doi.org/https://doi.org/10.1029/JD095iD02p01837, 1990.

Stewart, I. D. and Oke, T. R.: Local Climate Zones for Urban Temperature Studies, Bulletin of the American Meteorological Society, 93, 1879–1900, https://doi.org/10.1175/bams-d-11-00019.1, 2012.

Stockwell, W. R., Middleton, P., Chang, J. S., and Tang, X.: The second generation regional acid deposition model chemical mechanism for regional air quality modeling, Journal of Geophysical Research: Atmospheres, 95, 16 343–16 367, https://doi.org/https://doi.org/10.1029/JD095iD10p16343, 1990.

Tuccella, P., Curci, G., Visconti, G., Bessagnet, B., Menut, L., and Park, R. J.: Modeling of gas and aerosol with WRF/Chem over Europe: Evaluation and sensitivity study, Journal of Geophysical Research: Atmospheres, 117, https://doi.org/https://doi.org/10.1029/2011JD016302, 2011.

Venter, Z. S., Aunan, K., Chowdhury, S., and Lelieveld, J.: COVID-19 lockdowns cause global air pollution declines, Proceedings of the National Academy of Sciences, 117, 18 984–18 990, https://doi.org/10.1073/pnas.2006853117, 2020a.

Venter, Z. S., Aunan, K., Chowdhury, S., and Lelieveld, J.: COVID-19 lockdowns cause global air pollution declines, Proceedings of the National Academy of Sciences, 117, 18 984–18 990, https://doi.org/10.1073/pnas.2006853117, 2020b.

von Schneidemesser, E., Sibiya, B., Caseiro, A., Butler, T., Lawrence, M. G., Leitao, J., Lupascu, A., and Salvador, P.: Learning from the COVID-19 lockdown in berlin: Observations and modelling to support understanding policies to reduce NO2., Atmospheric Environment: X, 12, 100 122, https://doi.org/https://doi.org/10.1016/j.aeaoa.2021.100122, 2021.

Wang, H., Huang, C., Tao, W., Gao, Y., Wang, S., Jing, S., Wang, W., Yan, R., Wang, Q., An, J., Tian, J., Hu, Q., Lou, S., Pöschl, U., Cheng, Y., and Su, H.: Seasonality and reduced nitric oxide titration dominated ozone increase during COVID-19 lockdown in eastern China, npj Climate and Atmospheric Science, 5, https://doi.org/10.1038/s41612-022-00249-3, 2022.

Wang, W., van der A, R., Ding, J., van Weele, M., and Cheng, T.: Spatial and temporal changes of the ozone sensitivity in China based on satellite and ground-based observations, Atmospheric Chemistry and Physics, 21, 7253–7269, https://doi.org/10.5194/acp-21-7253-2021, 2021a.

Wang, Y., Zhu, S., Ma, J., Shen, J., Wang, P., Wang, P., and Zhang, H.: Enhanced atmospheric oxidation capacity and associated ozone increases during COVID-19 lockdown in the Yangtze River Delta, Science of The Total Environment, 768, 144 796, https://doi.org/https://doi.org/10.1016/j.scitotenv.2020.144796, 2021b.

Wesely, M.: Parameterization of surface resistances to gaseous dry deposition in regional-scale numerical models, Atmospheric Environment, 41, 52–63, https://doi.org/https://doi.org/10.1016/j.atmosenv.2007.10.058, 2007.

Wild, O.: Modelling the global tropospheric ozone budget: exploring the variability in current models, Atmospheric Chemistry and Physics, 7, 2643–2660, https://doi.org/10.5194/acp-7-2643-2007, 2007.

Wild, O., Zhu, X., and Prather, M. J.: Journal of Atmospheric Chemistry, 37, 245–282, https://doi.org/10.1023/a:1006415919030, 2000.

https://doi.org/10.5194/egusphere-2023-160
Preprint. Discussion started: 8 March 2023

Yang, L., Yuan, Z., Luo, H., Wang, Y., Xu, Y., Duan, Y., and Fu, Q.: Identification of long-term evolution of ozone sensitivity to precursors based on two-dimensional mutual verification, Science of The Total Environment, 760, 143 401, https://doi.org/https://doi.org/10.1016/j.scitotenv.2020.143401, 2021.

Yegorova, E. A., Allen, D. J., Loughner, C. P., Pickering, K. E., and Dickerson, R. R.: Characterization of an eastern U.S. severe air pollution episode using WRF/Chem, Journal of Geophysical Research: Atmospheres, 116, https://doi.org/https://doi.org/10.1029/2010JD015054, 2011.

Zhu, S., Poetzscher, J., Shen, J., Wang, S., Wang, P., and Zhang, H.: Comprehensive Insights Into Osub3/sub Changes During the COVID-19 From Osub3/sub Formation Regime and Atmospheric Oxidation Capacity, Geophysical Research Letters, 48, https://doi.org/10.1029/2021gl093668, 2021.

Zittis, G., Hadjinicolaou, P., Fnais, M., and Lelieveld, J.: Projected changes in heat wave characteristics in the eastern Mediterranean and the Middle East, Regional Environmental Change, 16, 1863–1876, https://doi.org/10.1007/s10113-014-0753-2, 2015.

https://doi.org/10.5194/egusphere-2023-160
Preprint. Discussion started: 8 March 2023

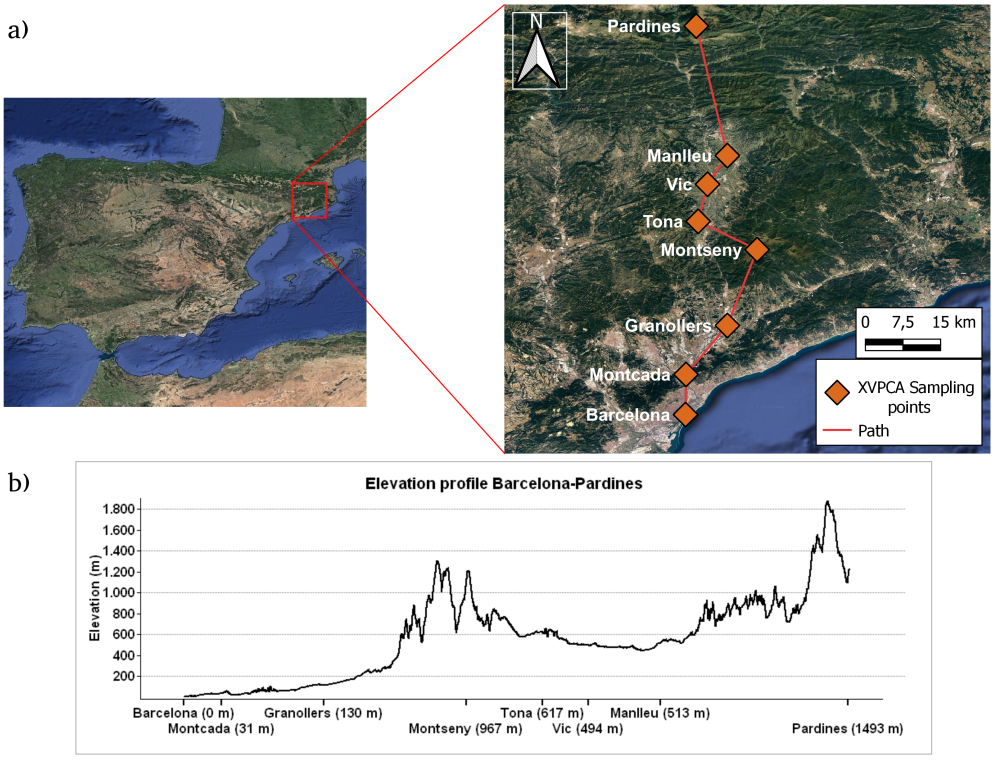

Figure 1. a) Location and b) main topographic features of the study area. Base maps in Panel a were taken from © Google Earth. The locations of air pollution monitoring stations (Xarxa de Vigilància i Previsió de la Contaminació Atmosfèrica, XVPCA) along the S–N axis (Barcelona-Vic Plain-Pyrenean range) are shown in Panel a (right).

https://doi.org/10.5194/egusphere-2023-160
Preprint. Discussion started: 8 March 2023

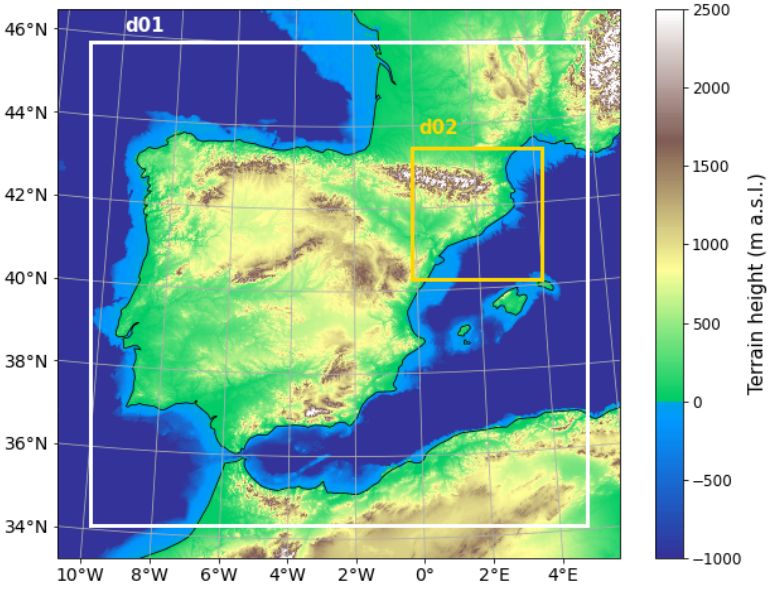

Figure 2. Model domains: D1: Iberian Peninsula 9 km x 9 km; D2: Catalonia horizontal resolution 3 km x 3 km.

https://doi.org/10.5194/egusphere-2023-160
Preprint. Discussion started: 8 March 2023

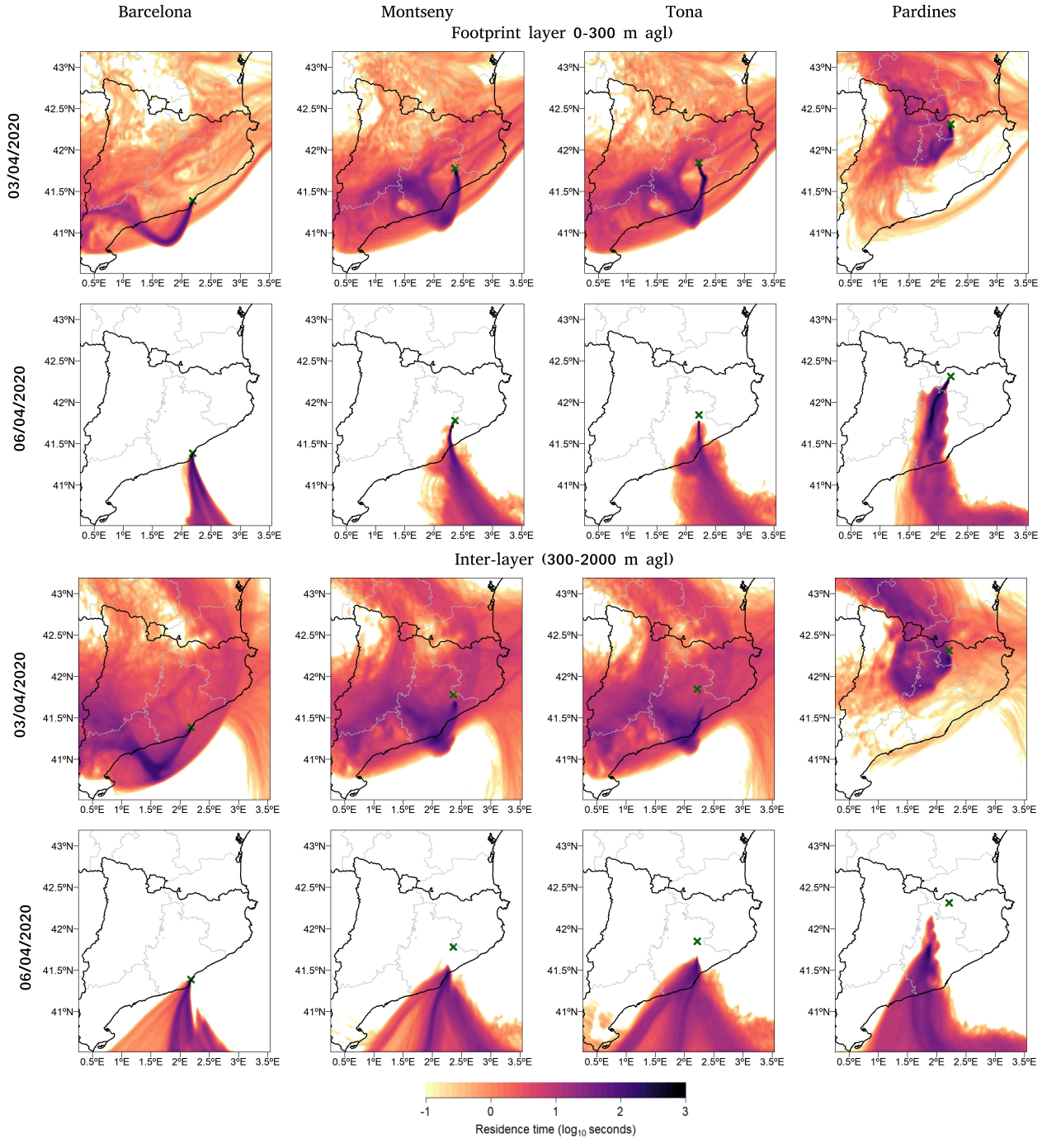

Figure 3. Simulated air parcel trajectories at the footprint layer (0-300 m agl, top panels) and interlayer (300-2000 m agl, bottom panels) for days 3 and 6 of April at 16 h at the four sites (from left to right): Barcelona, Montseny, Tona (Vic plain) and Pardines.

https://doi.org/10.5194/egusphere-2023-160
Preprint. Discussion started: 8 March 2023

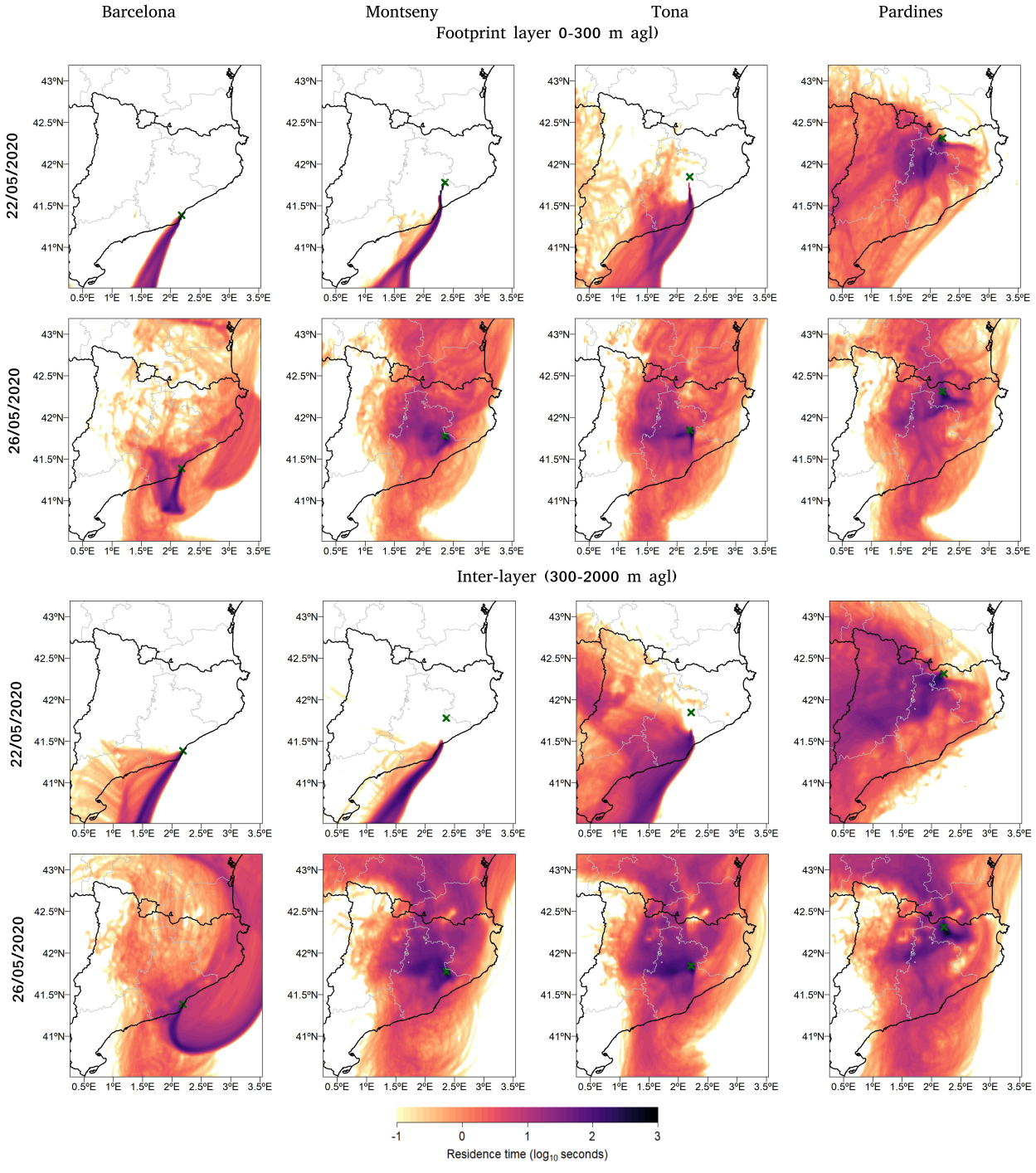

Figure 4. Same as Figure 3 for days 22 and 26 of May.

https://doi.org/10.5194/egusphere-2023-160
Preprint. Discussion started: 8 March 2023

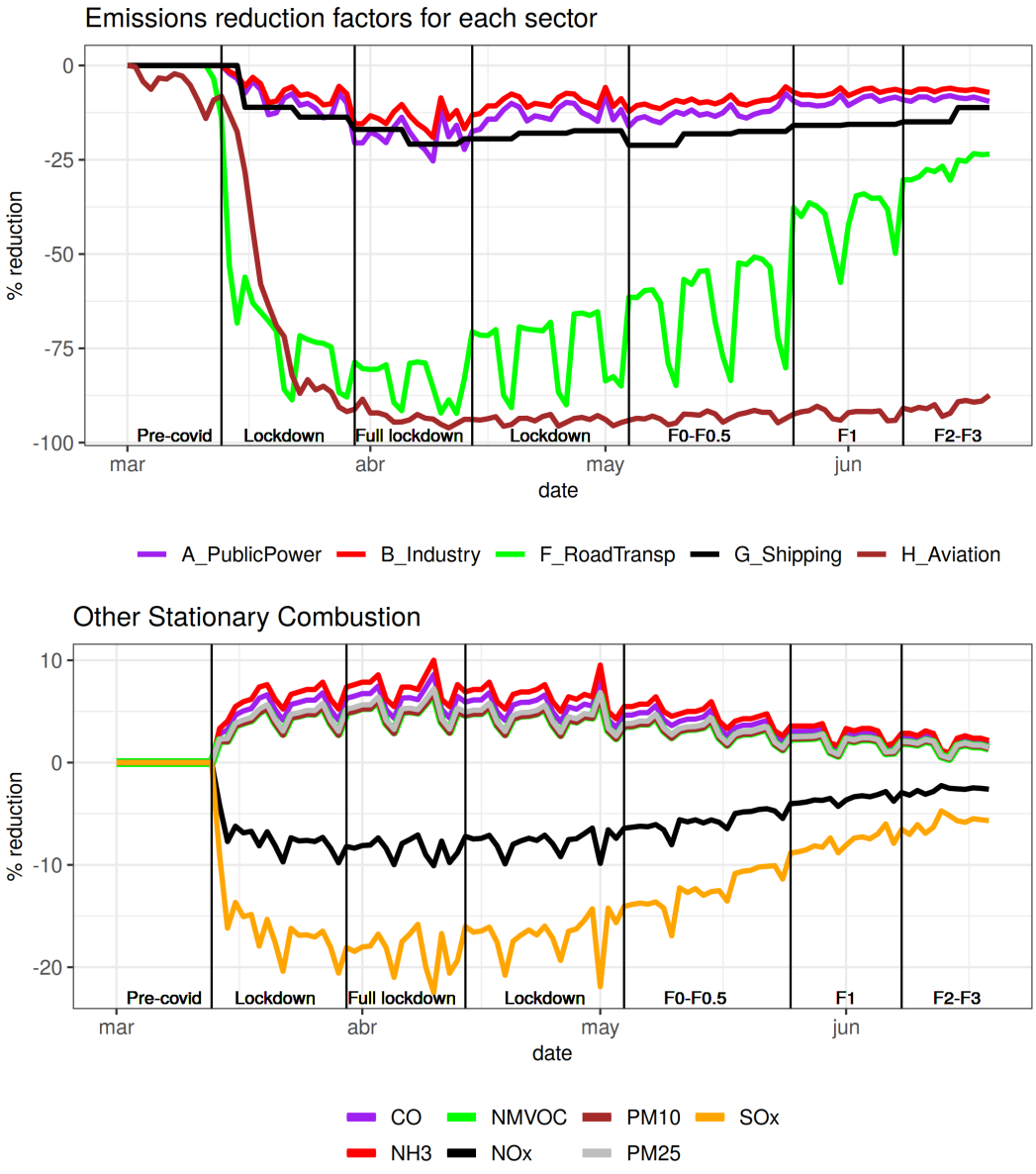

Figure 5. Emissions reduction percentage (%) for each sector. Note that the other stationary combustion sector has a different reduction level for each pollutant. The periods analysed here are written at the bottom of the figure.

https://doi.org/10.5194/egusphere-2023-160
Preprint. Discussion started: 8 March 2023

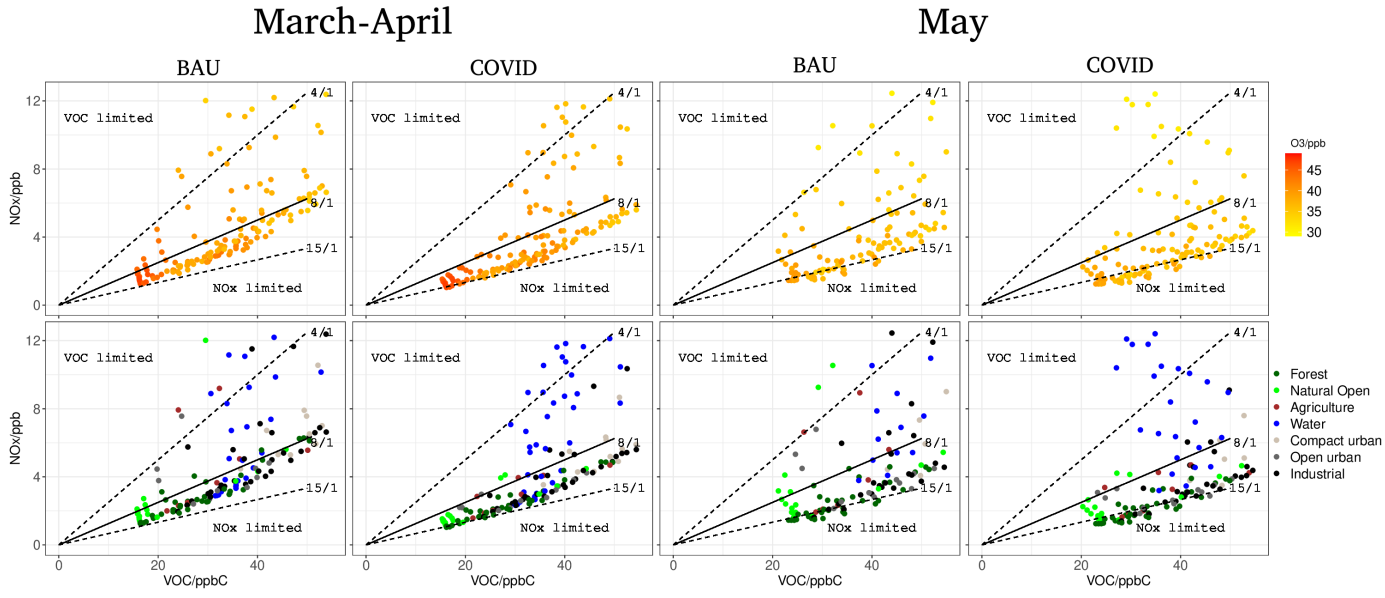

Figure 6. Change in O_3 concentrations (top panels) for 30 March to 12 April (only weekdays) and 18 to 30 May (only weekdays) for both simulations, BAU (left panels) and COVID (right panels), over the AMB area during the morning (6-8 UTC). The land use is also displayed for each grid (bottom panels).

https://doi.org/10.5194/egusphere-2023-160
Preprint. Discussion started: 8 March 2023

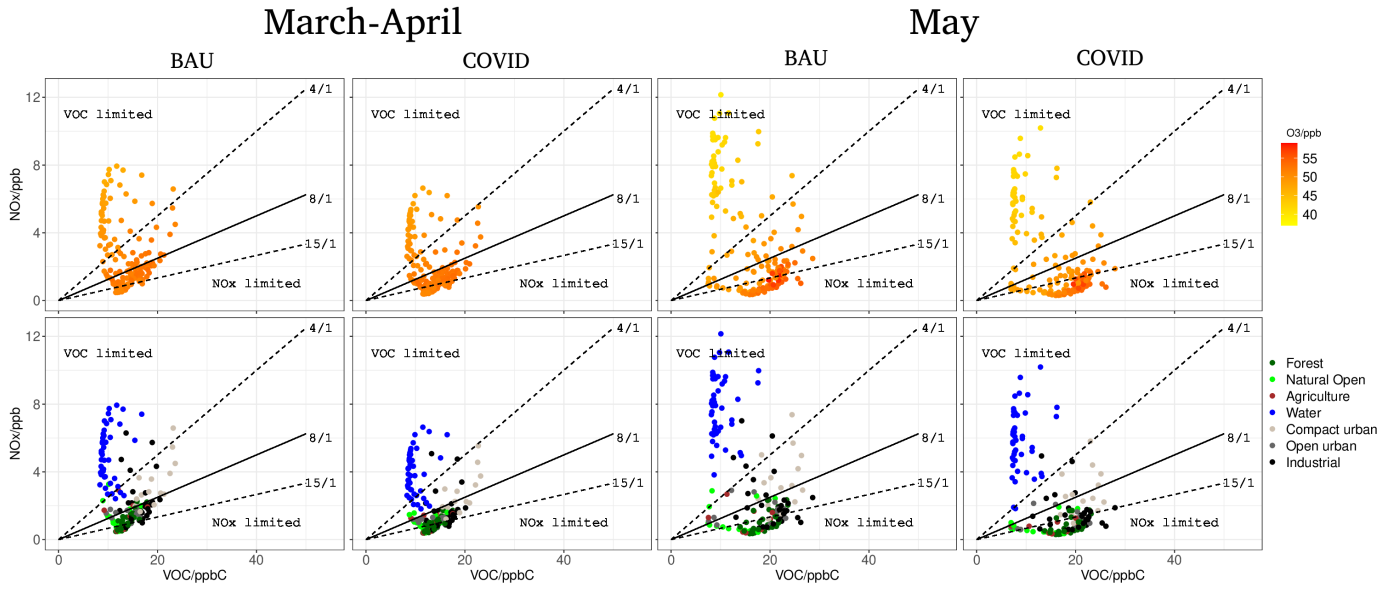

Figure 7. Same as Figure 6 during the afternoon (13-15 UTC).

https://doi.org/10.5194/egusphere-2023-160
Preprint. Discussion started: 8 March 2023

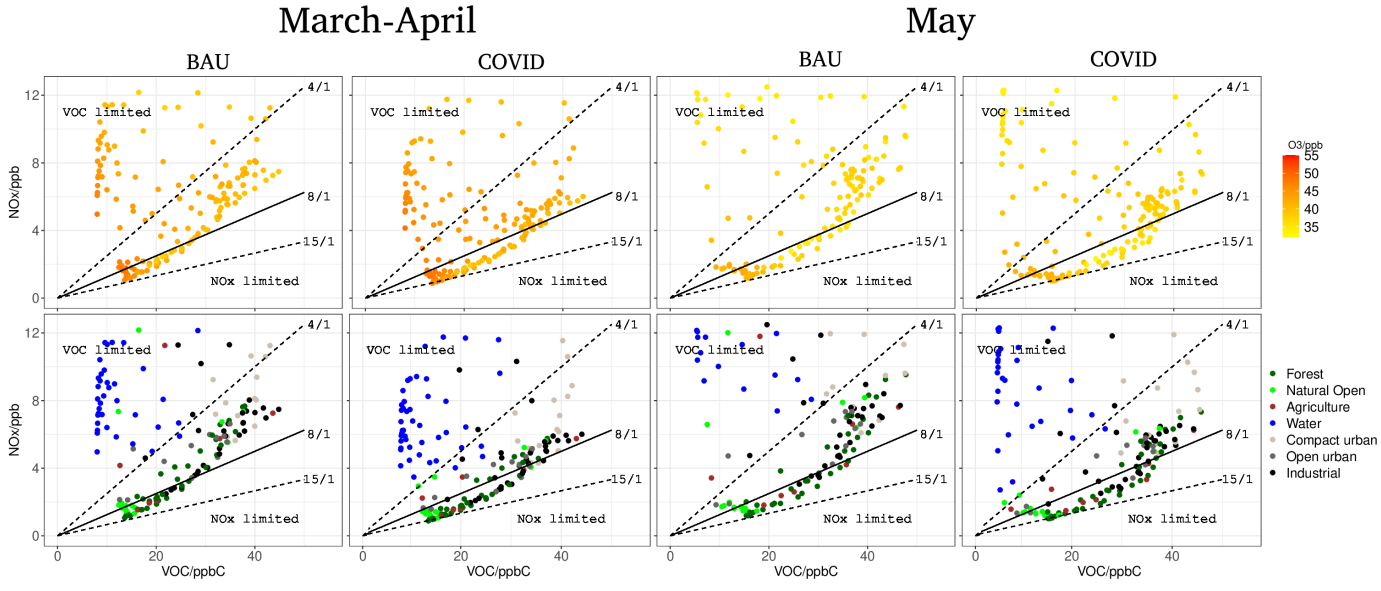

Figure 8. Same as Figure 6 during the evening (19-21 UTC).

https://doi.org/10.5194/egusphere-2023-160
Preprint. Discussion started: 8 March 2023

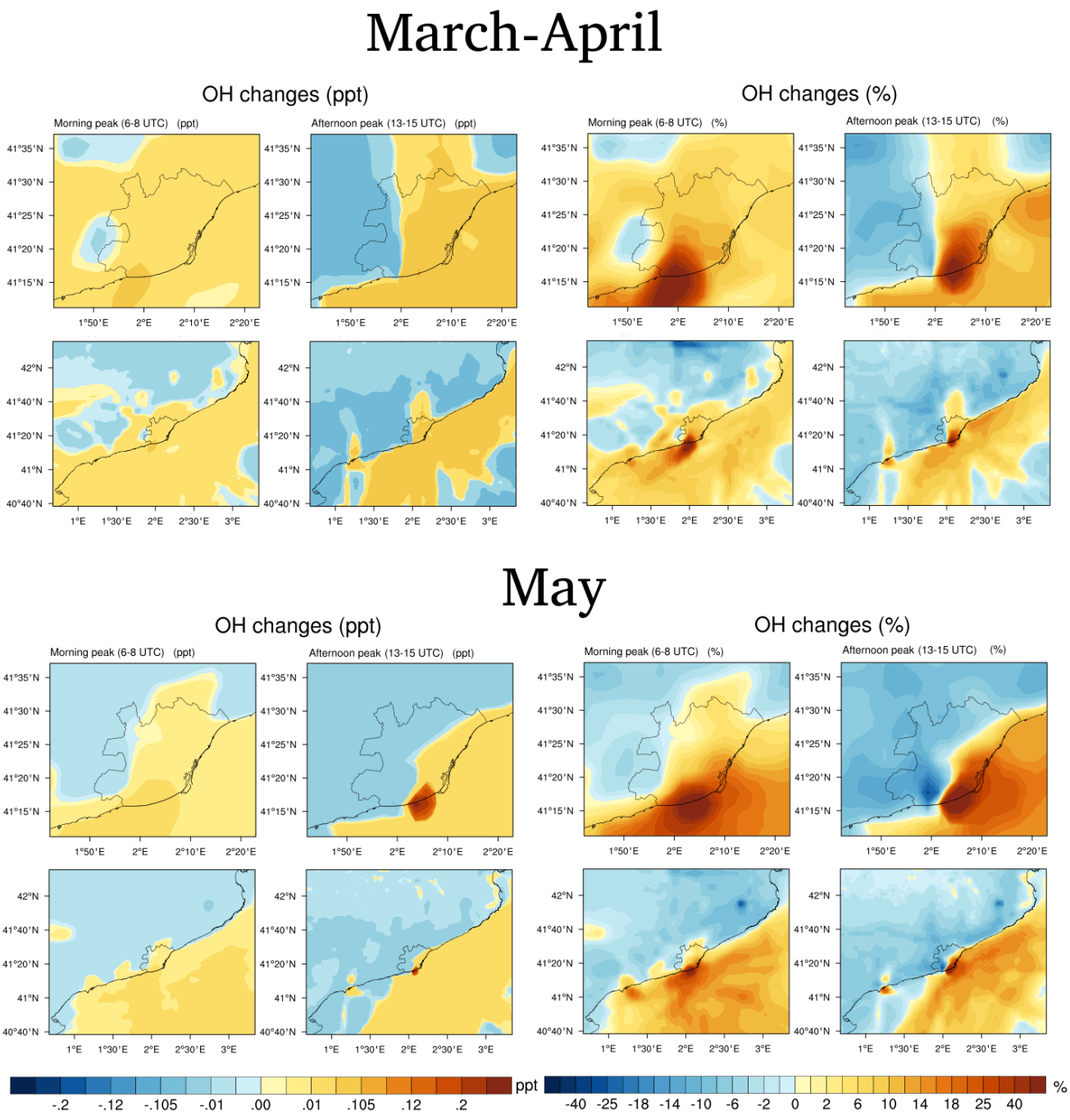

Figure 9. Morning and afternoon averaged OH changes over the Metropolitan Area of Barcelona (AMB) and the Catalonia region during 30 March to 12 April (only weekdays) and 18 to 30 May (only weekdays), with absolute values (ppt) and relative changes (%) shown. Relative changes (%) waswere calculated as ((COVID-BAU)/BAU)×100.

https://doi.org/10.5194/egusphere-2023-160
Preprint. Discussion started: 8 March 2023

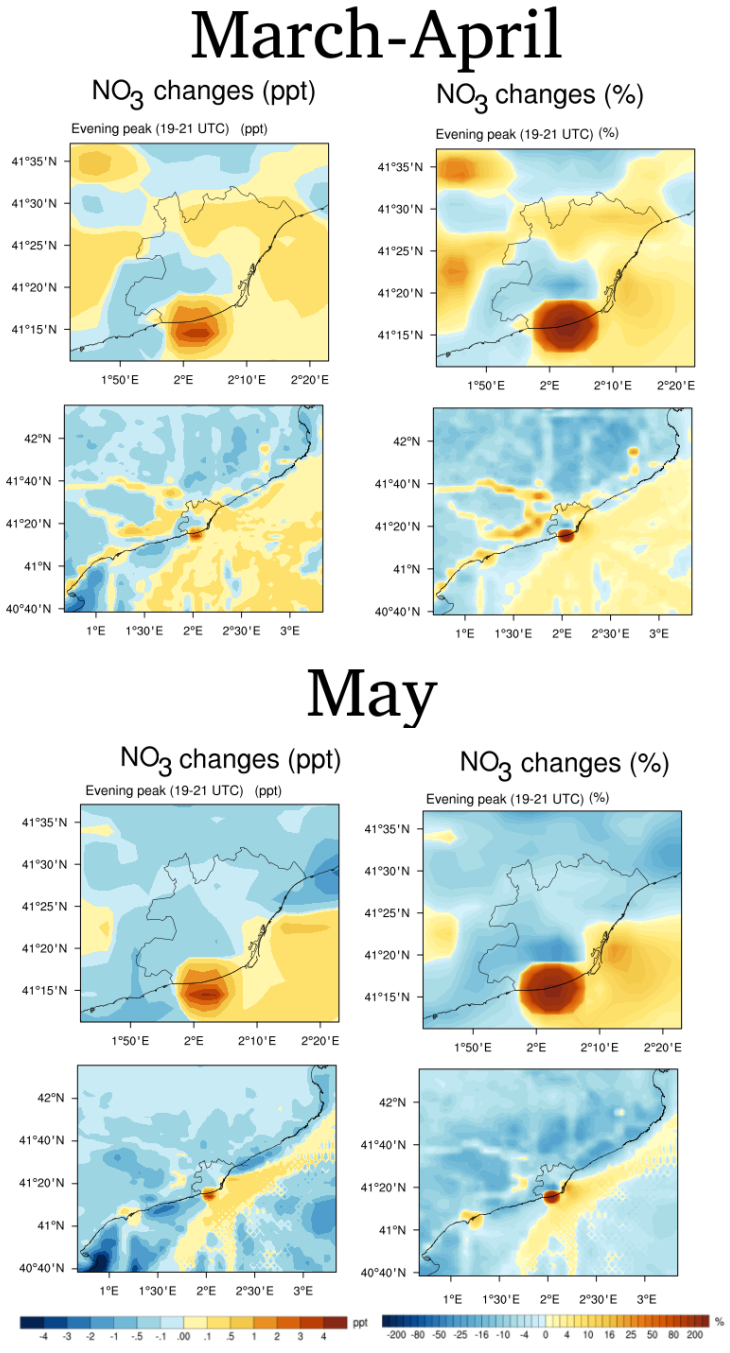

Figure 10. Evening-averaged NO_3 changes over the Metropolitan Area of Barcelona (AMB) and the Catalonia region during 30 March to 12 April (only weekdays) and 18 to 30 May (only weekdays), with absolute values (ppt) and relative changes (%) shown. Relative changes (%) were calculated as ((COVID-BAU)/BAU)×100.

https://doi.org/10.5194/egusphere-2023-160
Preprint. Discussion started: 8 March 2023

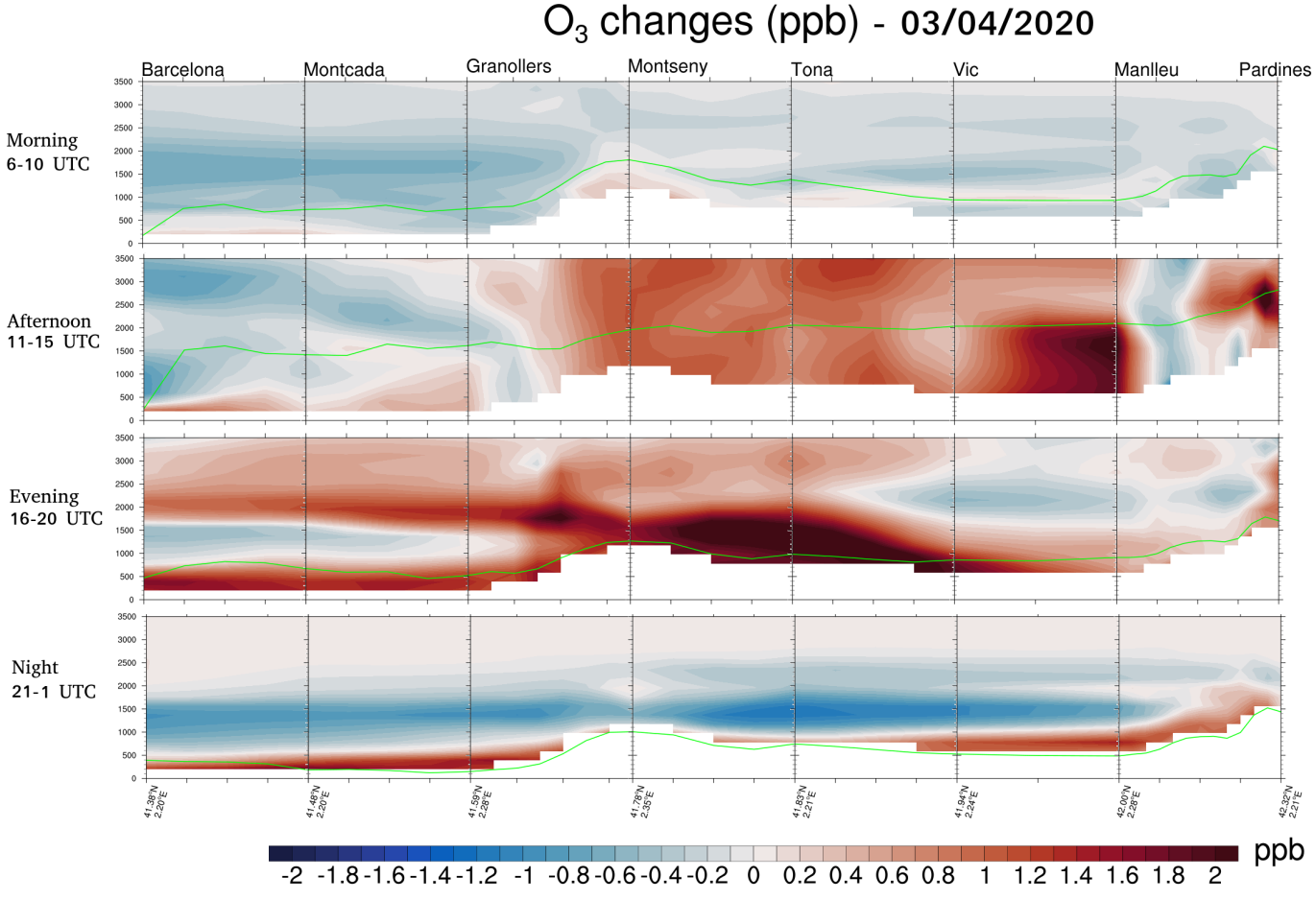

Figure 11. O_3 changes between the COVID and BAU simulations along the atmospheric plume from the AMB to the Pyrenees for the 3rd of April. The modelled PBLH is shown with a green line.

https://doi.org/10.5194/egusphere-2023-160
Preprint. Discussion started: 8 March 2023

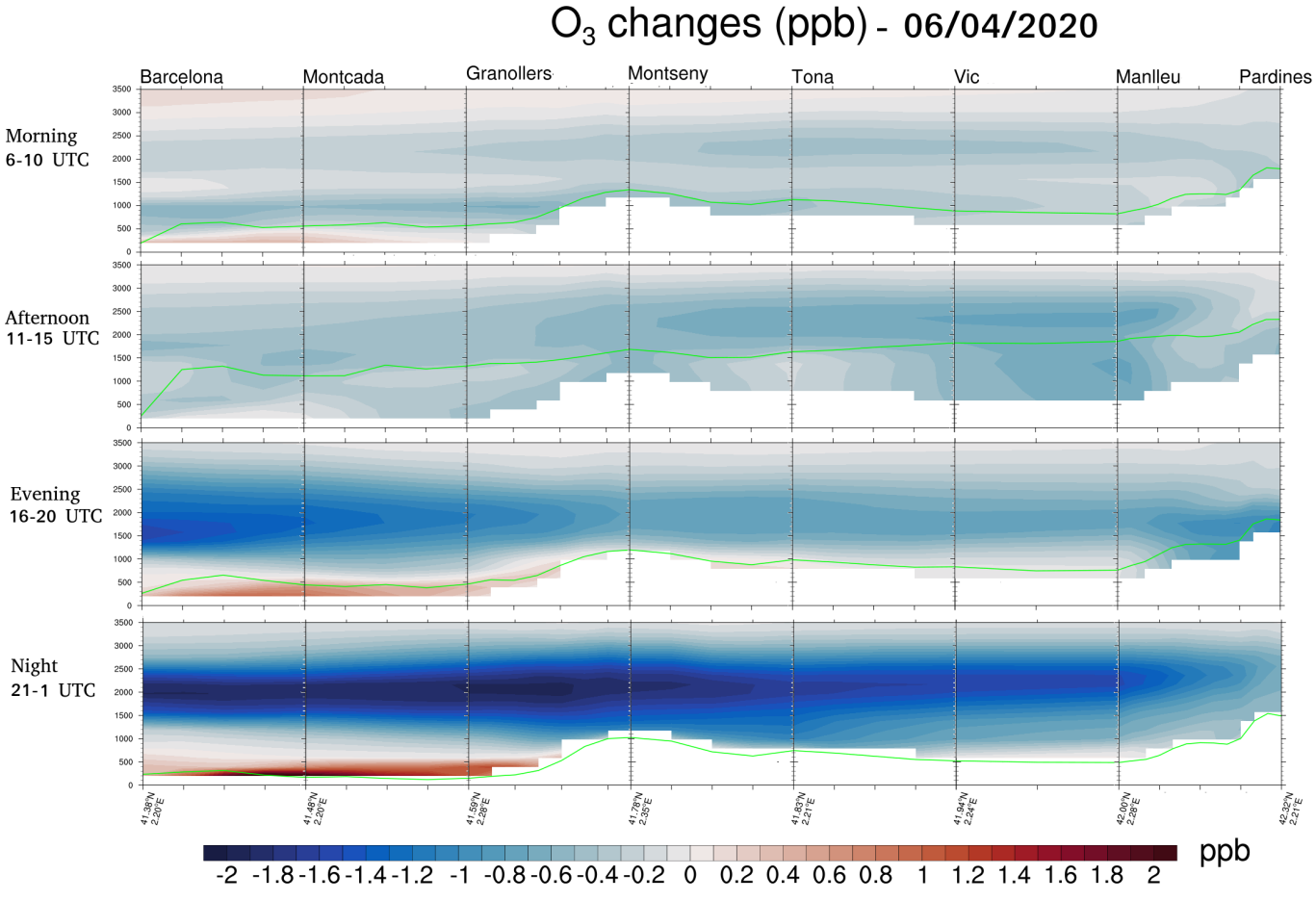

Figure 12. Same as Figure 11 for the 6th of April.

https://doi.org/10.5194/egusphere-2023-160
Preprint. Discussion started: 8 March 2023

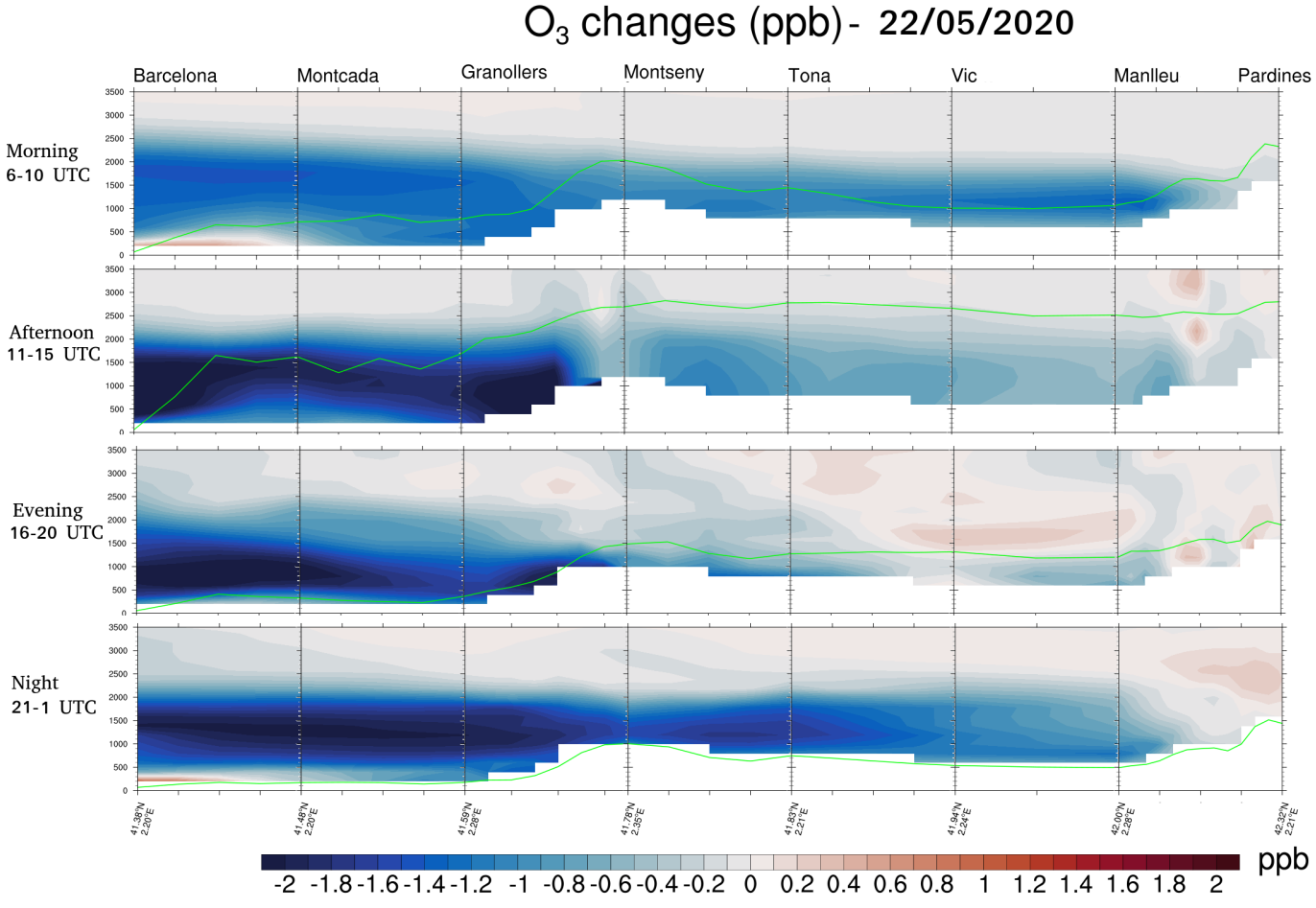

Figure 13. Same as Figure 11 for the 22nd of May.

https://doi.org/10.5194/egusphere-2023-160
Preprint. Discussion started: 8 March 2023

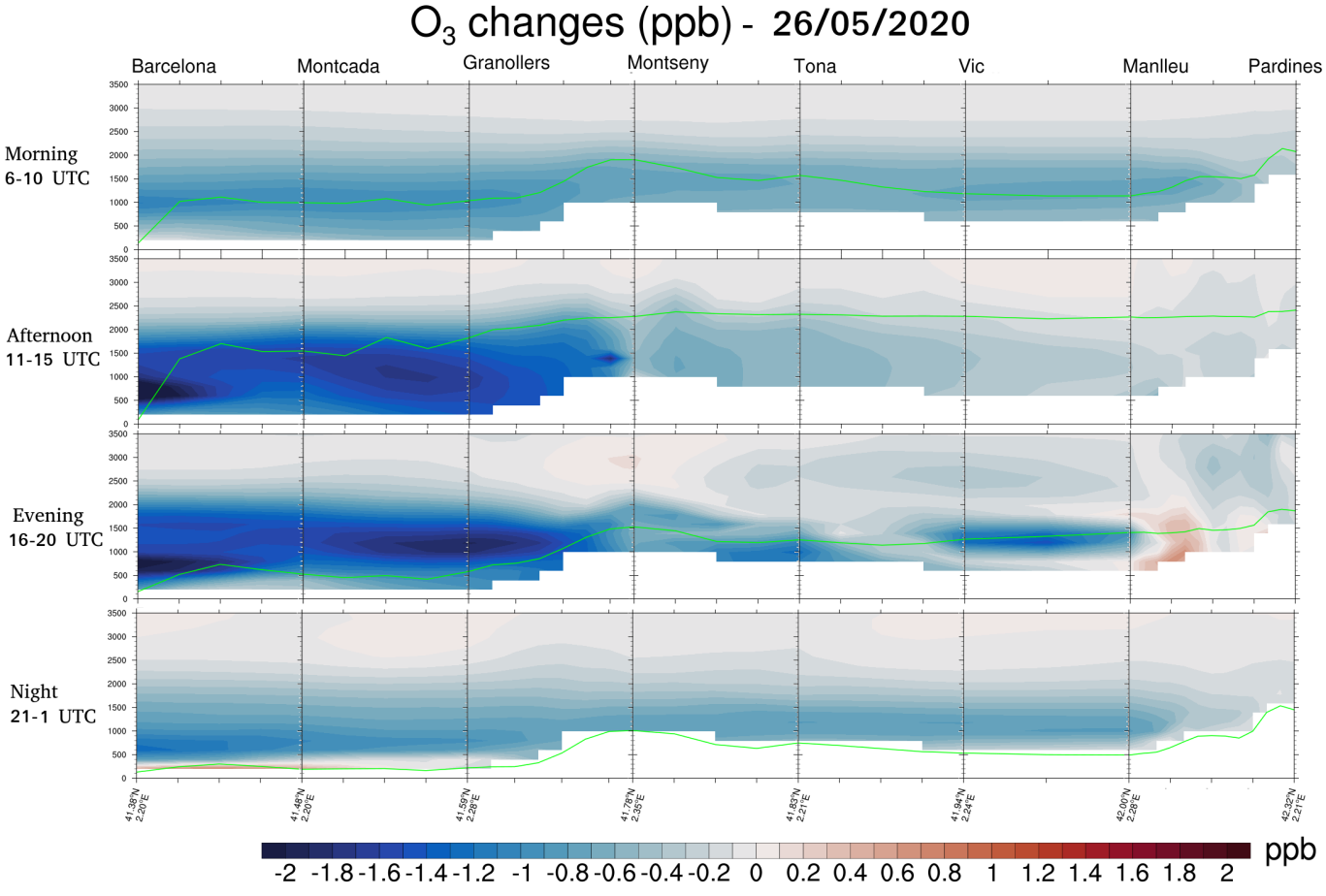

Figure 14. Same as Figure 11 for the 26th of May.

https://doi.org/10.5194/egusphere-2023-160
Preprint. Discussion started: 8 March 2023

Table 1. Meteorological conditions prevailing during the COVID-19 mobility restrictions (2020). The meteorological data were extracted from the following source: Servei Meteorològic de Catalunya (SMC). The circulation weather types (CWTs) were calculated by using the surface pressures of the NCEP/NCAR reanalysis dataset. CWTs: Cyclonic 56 (C), anticyclonic (A), pure advectives (N, S, E, W, NE, SE, NW, SW), hybrid cyclone advectives (CN, CNE, CE, CSE, CS, CSW, CW, CNW), hybrid anticyclone advectives (AN, ANE, AE, ASE, AS, ASW, AW, ANW). The mobility reduction over the AMB is provided in the 4th column (source: Google mobility reports (https://www.google.com/covid19/mobility/)).

Week	Dates (2020)	Stage	Mobility reduction	Psfc (hPa)	T (ºC)	Precipitation accumulated (mm)	CWTs
1	16-22/03	Lockdown	75.4%	1020,4	12,9	24,1	SE
2	23-29/03	Lockdown	82.2%	1015,8	11,4	20,4	E
3	30/03-05/04	Full Lockdown	84.4%	1015,9	11,6	25,3	C
4	06-12/04	Full Lockdown	84.4%	1023,0	15,0	0	A
5	13-19/04	Lockdown	82.6%	1014,5	15,1	109,1	U
6	20-26/04	Lockdown	79,8 %	1011,1	15,7	126,7	C
7	27/04-03/05	Lockdown	74%	1013,8	18,5	2,3	N
8	04-10/05	F0	60%	1014,0	19,3	6,9	U
9	11-17/05	F0	58,2%	1010,0	17,6	13,7	C
10	18-24/05	F0-F1	50,6%	1020,4	21,8	0,0	U
11	25-30/05	F1	43,2%	1021,0	20,8	4,6	E
12	01-07/06	F1-F2	41,4%	1009,5	19,8	21,9	U
13	08-14/06	F2	39%	1012,0	19,2	24,5	C
14	15-20/06	F2-F3	34,8%	1018,1	20,5	16,4	U

https://doi.org/10.5194/egusphere-2023-160
Preprint. Discussion started: 8 March 2023

Table 2. Model details and experiment configuration

Chemistry	
Chemical mechanism	RADM2 (Stockwell et al., 1990)
Aerosol scheme	MADE/SORGAM aerosol scheme (Ackermann et al., 1998; Schell et al., 2001)
Photolysis scheme	Fast-J (Wild et al., 2000)
Dry deposition	Wesely (2007)
Wet deposition	Grell and Dévényi (2002)
Anthropogenic emissions	CAMS-REG-APv3.1 database (Granier et al., 2019)
Biogenic emissions	MEGAN (Guenther et al., 2012)
Physics	
Urban canopy scheme	BEP+BEM (Salamanca et al., 2011)
PBL scheme	BouLac (Bougeault and Lacarrere, 1989)
Resolution and Initial conditions	
Horizontal resolution	D1: 9 km×9 km, D2: 3km x 3km
Vertical layers	45
Top of the atmosphere	100 hPa
Chemical initial condition	WACCM (Gettelman et al., 2019)
Meteorological initial condition	ERA5 (Hersbach et al., 2020)
Chemistry spin-up	1 month

https://doi.org/10.5194/egusphere-2023-160
Preprint. Discussion started: 8 March 2023

Table 3. Averages NO_x/VOC ratio and ozone concentrations from 30 March to 12 April (only weekdays) and 18 to 30 May (only weekdays) in the morning (6-8 UTC), afternoon (13-15 UTC) and evening (19-21 UTC). Red and blue cells indicate VOCs and NO_x regimes, respectively. The relative changes in ozone concentrations (%) are shown in brackets and were calculated as ((COVID-BAU)/BAU)×100.

March-April	Landuse	Morning		Afternoon		Evening	
		BAU	COVID	BAU	COVID	BAU	COVID
[NO_x/VOC]	Forest	0.102	0.083	0.073	0.059	0.143	0.111
	Natural Open	0.158	0.098	0.109	0.077	0.194	0.122
	Agriculture	0.156	0.100	0.113	0.077	0.195	0.101
	Water	0.25	0.201	0.495	0.393	0.707	0.535
	Compact urban	0.166	0.139	0.171	0.137	0.236	0.184
	Open urban	0.125	0.088	0.108	0.081	0.182	0.135
	Industrial	0.149	0.120	0.135	0.100	0.215	0.151
O_3 (ppb)	Forest	40.3	40.7 (1.0 %)	51.7	51.7 (0.0 %)	42.3	42.9 (1.3 %)
	Natural Open	42.8	43.9 (2.5 %)	51.7	51.9 (0.3 %)	45.4	46.4 (2.1 %)
	Agriculture	37.3	38.5 (3.4 %)	51	51.2 (0.4%)	40.7	42.2 (3.7 %)
	Water	37	38.7 (4.6 %)	48.6	49.4 (1.6 %)	42.1	44.2 (5.0 %)
	Compact urban	35.8	36.9 (2.9 %)	52	52.3 (0.6 %)	40.4	42.2 (4.3 %)
	Open urban	39.4	40.4 (2.4 %)	52.6	52.8 (0.3 %)	42.6	43.6 (2.4 %)
	Industrial	36.8	37.7 (2.3 %)	52.2	52.5 (0.5 %)	40.1	41.8 (4.2 %)

May	Landuse	Morning		Afternoon		Evening	
		BAU	COVID	BAU	COVID	BAU	COVID
[NO_x/VOC]	Forest	0.076	0.066	0.053	0.043	0.139	0.115
	Natural Open	0.122	0.087	0.078	0.052	0.194	0.129
	Agriculture	0.122	0.090	0.077	0.046	0.192	0.118
	Water	0.349	0.279	0.792	0.663	1.327	1.028
	Compact urban	0.137	0.121	0.156	0.125	0.261	0.210
	Open urban	0.101	0.078	0.099	0.072	0.191	0.150
	Industrial	0.125	0.104	0.107	0.075	0.230	0.165
O_3 (ppb)	Forest	36.9	36.7 (-0.6 %)	51.3	50.5 (-1.6 %)	37.7	37.6 (-0.1 %)
	Natural Open	37.0	37.3 (0.6 %)	48.9	48.3 (-1.3 %)	40.3	40.6 (0.8 %)
	Agriculture	33.3	33.8 (1.4 %)	50.5	49.9 (-1.2 %)	36.3	37.3 (3.0 %)
	Water	29.7	31.2 (4.9 %)	42.5	43.4 (2.2 %)	32.0	35 (9.4 %)
	Compact urban	33.6	33.9 (1.0 %)	50.8	50.4 (-0.8 %)	35.8	37.2 (3.8 %)
	Open urban	36.7	36.9 (0.5 %)	51.3	50.7 (-1.1 %)	38.2	38.6 (1.1 %)
	Industrial	34.3	34.6 (0.9 %)	52.1	51.6 (-1.1 %)	36.3	37.6 (3.5 %)